



**HAL**  
open science

## RAFT synthesis of well-defined PVDF-b-PVAc block copolymers

Marc Guerre, S. M. Wahidur Rahaman, Bruno Ameduri, Rinaldo Poli,  
Vincent Ladmiral

► **To cite this version:**

Marc Guerre, S. M. Wahidur Rahaman, Bruno Ameduri, Rinaldo Poli, Vincent Ladmiral. RAFT synthesis of well-defined PVDF-b-PVAc block copolymers. *Polymer Chemistry*, 2016, 7 (45), pp.6918 - 6933. 10.1039/c6py01247g . hal-01398180

**HAL Id: hal-01398180**

**<https://hal.science/hal-01398180>**

Submitted on 1 Mar 2021

**HAL** is a multi-disciplinary open access archive for the deposit and dissemination of scientific research documents, whether they are published or not. The documents may come from teaching and research institutions in France or abroad, or from public or private research centers.

L'archive ouverte pluridisciplinaire **HAL**, est destinée au dépôt et à la diffusion de documents scientifiques de niveau recherche, publiés ou non, émanant des établissements d'enseignement et de recherche français ou étrangers, des laboratoires publics ou privés.

RAFT Synthesis of Well-Defined PVDF-*b*-PVAc Block CopolymersMarc Guerre,<sup>a</sup> S. M. Wahidur Rahaman,<sup>b</sup> Bruno Ameduri, Rinaldo Poli<sup>b,\*</sup> Vincent Ladmiral<sup>a,\*</sup>Received 00th January 20xx,  
Accepted 00th January 20xx

DOI: 10.1039/x0xx00000x

www.rsc.org/

RAFT polymerization of Vinylidene Fluoride (VDF), leading to relatively well-defined poly(vinylidene fluoride) (PVDF), is negatively affected by chain inversion resulting in less easily reactivatable PVDF-*XA* dormant chains (terminated with the tail end of an inversely added VDF unit; *XA* = xanthate moiety). Although slow reactivation of these chains by PVDF<sup>\*</sup> radicals (in contrast to general belief) was recently demonstrated, slow radical exchange leads to progressive loss of the chain growth control. The present article deals with the possibility of synthesizing block copolymers from PVDF-*XA* macroCTAs by sequential addition. The investigations show that only PVDF<sub>H</sub>-*XA* (chains terminated with the head end of regularly added VDF) can be reactivated by PNVP<sup>\*</sup> (poly(*N*-vinylpyrrolidone) radicals and that PVDF<sub>T</sub>-*XA* chains are completely unreactive in the presence of PNVP<sup>\*</sup>, PBA<sup>\*</sup> (poly(butylacrylate)) or PDMA<sup>\*</sup> (poly(*N,N'*-dimethylacrylamide)). However, both PVDF<sub>H</sub>-*XA* and PVDF<sub>T</sub>-*XA* can be reactivated by PVAc<sup>\*</sup> (poly(vinyl acetate)) radicals. The reactivation of the PVDF<sub>T</sub>-*XA*, albeit slower than that of the PVDF<sub>H</sub>-*XA*, is sufficiently fast to allow the synthesis of unprecedented well-defined PVDF-*b*-PVAc block copolymers with relatively high end-group fidelity. DFT calculations rationalize this behavior on the basis of faster radical exchange in the order PVDF<sub>H</sub>*XA*/VAc > PVDF<sub>H</sub>-*XA*/NVP > PVDF<sub>T</sub>-*XA*/VAc >> PVDF<sub>T</sub>-*XA*/NVP. Success of the chain extension also relies on faster activation relative to homopropagation of the chain extending monomer, as well as fast addition to the released PVDF<sub>H</sub><sup>\*</sup> and PVDF<sub>H</sub><sup>\*</sup> to the new monomer.

## Introduction

Owing to its remarkable thermal, chemical and electroactive properties,<sup>1-3</sup> poly(vinylidene fluoride) (PVDF) is a very important fluorinated polymer. The radical polymerization of VDF is relatively well-known, but the use of reversible deactivation radical polymerization (RDRP) techniques to prepare well-defined PVDF is still a very challenging topic in fluorinated polymer chemistry.<sup>4</sup> Iodine transfer polymerization (ITP), also known as iodine degenerative transfer (IDT) has been relatively well studied over the last two decades but, in spite of its simplicity, affords only moderate control in VDF polymerization.<sup>5-7</sup> Recently, our team has made an important contribution to VDF RDRP<sup>8,9</sup> with a thorough study of VDF RAFT<sup>10-12</sup> polymerization. Similarly to what Asandei showed for ITP,<sup>13</sup> this study revealed that VDF head-to-head additions lead to the accumulation of much less reactive -CF<sub>2</sub>-CH<sub>2</sub>-*XA* (where *XA* stands for xanthate) terminated PVDF chains resulting in broader molar mass distributions, difficulties to synthesize block copolymers, and limiting the accessible range of molar masses. Moreover, the occurrence of transfer reactions (mainly from the CF<sub>2</sub><sup>\*</sup> radical to the solvent), which cause a 10% loss in chain-end functionality and consumption of a significant amount of chain transfer agent (CTA), was also demonstrated.<sup>8</sup> Nonetheless, RAFT is, so far, arguably the best technique to synthesize PVDF with good control and relatively high chain-end

functionality. This technique was also shown to open the way to the preparation of well-defined PVDF-based architectures.<sup>14</sup> A crucial step towards more sophisticated architectures is the preparation of well-defined diblock copolymers.<sup>15</sup> The first studies on PVDF-containing block copolymers described the use of brominated PVDF telomers as macroinitiator for the ATRP of styrene<sup>16</sup> or that of iodine terminated PVDF for the ATRP of MMA.<sup>17</sup> In both cases, relatively broad and bimodal molar mass distributions (ca. 1.6) were observed. A few articles dealing with the synthesis of PVDF based block architectures using telomerization<sup>18-21</sup> and free radical polymerization from functionalized initiators<sup>22-25</sup> were then published. PVDF telomerization resulted in very limited degree of polymerization and broad dispersities were observed in the case of peroxide initiated radical polymerization. ITP<sup>26-27</sup> has extensively been studied for the synthesis of PVDF containing block copolymers. Pioneered at Daikin in the late 70 s, this process led to the production of fluorinated block copolymers as commercial products. Valade et al.<sup>28</sup> attempted the synthesis of PVDF-*b*-PS block copolymer by sequential addition of VDF and styrene on a fluorinated alkyl iodide. However, broad dispersity (1.8-2.0) and a bimodal GPC trace were observed due to the presence of -CF<sub>2</sub>-CH<sub>2</sub>-I end groups which did not reactivate efficiently during the polymerization of styrene. This phenomenon was also identified in other articles dealing with the ITP of VDF.<sup>6,29</sup> In particular, Asandei's group<sup>7,30,31</sup> recently demonstrated that the addition of Mn<sub>2</sub>(CO)<sub>10</sub> to the photomediated ITP of VDF offers an elegant solution to this problem. In-situ generated Mn(CO)<sub>5</sub><sup>\*</sup> radicals reactivate all the iodine-terminated chains and thus affords purer block copolymers (i.e. block copolymers devoid of contamination from PVDF homopolymer chains). However, the second block is synthesized under free radical polymerization conditions and broad dispersity are obtained. RAFT was also

<sup>a</sup>Institut Charles Gerhardt Montpellier UMR5253 CNRS-UM-ENSCM – Equipe Ingénierie et Architectures Macromoléculaires, Montpellier, France. E-mail: vincent.ladmiral@enscm.fr

<sup>b</sup>CNRS, LCC (Laboratoire de Chimie de Coordination), Université de Toulouse, UPS, INPT, 205 Route de Narbonne, BP 44099, F-31077 Toulouse Cedex 4, France. † Electronic Supplementary Information (ESI) available: [details of any supplementary information available should be included here]. See DOI: 10.1039/x0xx00000x

used to prepare VDF-containing block copolymers<sup>32-34</sup> with moderate success, probably because of partial reactivation of the end-groups as in ITP.

We recently reported that the reputedly completely unreactive PVDF-CF<sub>2</sub>-CH<sub>2</sub>-XA (PVDF<sub>T</sub>-XA) chains are actually reactivated, albeit at a slower rate than the PVDF-CH<sub>2</sub>-CF<sub>2</sub>-XA (PVDF<sub>H</sub>-XA) chains, by PVDF<sup>•</sup> radicals.<sup>35</sup> That study demonstrated that the VDF RAFT polymerization proceeds via two regimes: a first stage where PVDF<sub>H</sub>-XA are still present, with good chain growth control; and a second stage when all the dormant chains have been transformed into PVDF<sub>T</sub>-XA, for which transfer with PVDF<sup>•</sup> radicals is slower than propagation leading to very poor control. The present study examines the phenomena at work in the block extension of RAFT synthesized PVDF<sup>8</sup> with a range of vinyl monomers including vinyl acetate (VAc) and reports the surprising synthesis of well-defined PVDF-*b*-PVAc block copolymers by sequential monomer addition. The analysis of the radical exchange process on the xanthate transfer agent and of the radical addition to monomer, carried out by DFT calculations on suitable molecular model systems, provides a framework of understanding and allows rationalizing this unexpected result.

## Experimental

### Materials and Methods

All reagents were used as received unless stated otherwise. 1,1-Difluoroethylene (vinylidene fluoride, VDF) was kindly supplied by Arkema (Pierre-Benite, France). O-ethyl-S-(1-methoxycarbonyl)ethylthiocarbonate (CTA<sub>XA</sub>) was synthesized according to the method described by Liu et al.<sup>36</sup> Tert-amyl peroxy-2-ethylhexanoate (Trigonox 121, purity 95%) was purchased from AkzoNobel (Chalons-sur-Marne, France). ReagentPlus grade (purity > 99%) 2,2-azoisobutyronitrile (AIBN), vinyl acetate (VAc), butyl acrylate (BA), N-vinylpyrrolidone (NVP), N,N-dimethylacrylamide (DMA), dimethyl carbonate (DMC), dimethylformamide (DMF), acetonitrile (ACN), tetrahydrofuran, (THF), methanol (MeOH), and laboratory reagent grade hexane (purity > 95%) were purchased from Sigma Aldrich and used as received. AIBN was purified by recrystallization from methanol twice before use.

### Nuclear Magnetic Resonance (NMR)

The Nuclear Magnetic Resonance (NMR) spectra were recorded on a Bruker AC 400 instrument. Deuterated acetone or DMSO was used as the solvent in each sample. Coupling constants and chemical shifts are given in Hertz (Hz) and parts per million (ppm), respectively. The experimental conditions for recording <sup>1</sup>H and <sup>19</sup>F NMR spectra were as follows: flip angle 90° (or 30°), acquisition time 4.5 s (or 0.7 s), pulse delay 2 s (or 2 s), number of scans 128 (or 512), and a pulse width of 5 μs for <sup>19</sup>F NMR. In situ NMR experiments were recorded with a pulse delay of 1 s, acquisition times of 4 s and 0.87 s, and 8 and 16 scans for <sup>1</sup>H and <sup>19</sup>F NMR, respectively.

### Size Exclusion Chromatography

Size exclusion chromatograms (SEC) were recorded using a triple detection GPC from Agilent Technologies with its

corresponding Agilent software, dedicated to multi-detector GPC calculation. The system used two PL1113-6300 ResiPore 300 x 7.5 mm columns with DMF (containing 0.1 wt % of LiCl) as the eluent with a flow rate of 0.8 mL·min<sup>-1</sup> and toluene as flow rate marker. The detector suite comprised a PL0390-0605390 LC light scattering detector with 2 diffusion angles (15° and 90°), a PL0390-06034 capillary viscosimeter, and a 390-LC PL0390-0601 refractive index detector. The entire SEC-HPLC system was thermostated at 35°C. PMMA standards were used for the calibration. The typical sample concentration was 10 mg/mL.

### Differential Scanning Calorimetry

DSC measurements were performed on 10-15 mg samples on a Netzsch DSC 200 F3 instrument using the following heating/cooling cycle: cooling from room temperature (ca. 20 °C) to -50 °C at 20 °C/min, isotherm plateau at -50 °C for 5 min, first heating ramp from -50 to 200 °C at 10 °C/min, cooling stage from 200 to -50 °C at 10 °C/min, isotherm plateau at -50 °C for 3 min, second heating ramp from -50 °C to 200 °C at 10 °C/min and last cooling stage from 200 °C to room temperature (ca. 20 °C). The instrument was calibrated with noble metals and checked before analysis with an indium sample. Melting points were determined at the maximum of the enthalpy peaks.

### Thermogravimetric Analyses

TGA analyses were carried out on 10-15 mg samples on a TGA Q50 apparatus from TA Instruments from 20 °C to 580 °C, in platinum pans, at a heating rate of 10 °C min<sup>-1</sup>, in air. A thermal degradation temperature at 5% weight loss (T<sub>d</sub> 5%) was arbitrarily chosen.

### Autoclave

The polymerizations of VDF were performed in a 100 mL Hastelloy Parr autoclave systems (HC 276), equipped with a mechanical Hastelloy stirring system, a rupture disk (3000 PSI), inlet and outlet valves, and a Parr electronic controller to regulate the stirring speed and the heating. Prior to reaction, the autoclave was pressurized with 30 bars of nitrogen to check for leaks. The autoclave was then put under vacuum (20·10<sup>-3</sup> bar) for 30 minutes to remove any trace of oxygen. A degassed solution of initiator and CTA<sub>XA</sub> was introduced via a funnel under vacuum. The reactor was then cooled using a liquid nitrogen bath and VDF was transferred by double weighing (i.e. mass difference before and after filling the autoclave with VDF). After warming to ambient temperature, the autoclave was heated to the target temperature under mechanical stirring.

### Syntheses

MacroRAFT PVDF-XA with the characteristics listed in Table 1 (entry 1-3) were generated on the basis of previously published protocols.<sup>8,9,35</sup> The synthetic details and the equations used to determine the proportion of each chain ends (PVDF<sub>T</sub>-XA, PVDF<sub>H</sub>-XA and PVDF-H) are reported in the Supporting Information. All the Proportions reported in this article are in mol %.

### RAFT Polymerization of Vac

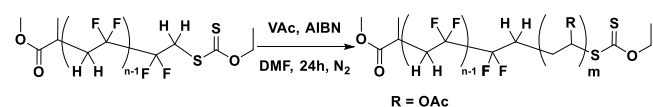
In a 50 mL round bottom flask, O-ethyl-S-(1-methoxycarbonyl)ethylthiocarbonate (1.613 g, 7.744 · 10<sup>-3</sup> mol) and AIBN (0.254 g, 1.55 · 10<sup>-3</sup> mol) were dissolved in 25 mL of anhydrous ACN and the solution was degassed by N<sub>2</sub> bubbling

during 15 min. A degassed solution of VAc (20.0 g, 2.32  $10^{-1}$  mol) was then introduced in the reaction vessel and the reaction medium was left under vigorously stirring at 60°C for 14 hours. ACN was then removed under vacuum; the viscous residue was then dissolved in 20 mL of acetone and precipitated from chilled hexane. The resulting polymer was dried until constant weight under vacuum at 50°C to remove traces of solvent (yield = 73 %) (entry 4, Table 1).

$^1\text{H}$  NMR (400 MHz ( $\text{CD}_3$ ) $_2\text{CO}$ ,  $\delta$  (ppm)): 1.06-1.17 (-CH( $\text{CH}_3$ )(C=O)-), 1.37-1.46 (-S(C=S)O-CH $_2$ -CH $_3$ ), 1.68-1.91 (-CH(OAc)-CH $_2$ -CH(OAc)-), 1.91-2.04 (-CH(OAc)-), 2.16-2.35 (-CH $_2$ -CH(OAc)-S(C=S)OEt), 2.38-2.62 (-CH( $\text{CH}_3$ )(C=O)-O-CH $_3$ ), 3.18-3.51 (-CH(OAc)-CH $_2$ -S(C=S)OEt), 3.56-3.74 (-CH( $\text{CH}_3$ )-(C=O)-O-CH $_3$ ), 3.95-4.13 (-CH $_2$ -(CH $_3$ (C=O)O)CH $_2$ ), 4.57-4.75 (-S(C=S)O-CH $_2$ -CH $_3$ ), 4.76-5.14 (-CH $_2$ -CH(OAc)-CH $_2$ -), 5.13-5.24 (-CH(OAc)-CH $_2$ -S(C=S)OEt), 6.50-6.70 (-CH $_2$ -CH(OAc)-S(C=S)OEt).

#### Synthesis of PVDF-*b*-PVAc block copolymers using PVDF-XA as MacroCTA.

A typical synthesis of a PVDF-*b*-PVAc block copolymer was performed as follows (Scheme 1): PVDF-XA macroCTA (entry 1, Table 1) (1.00 g, 3.33  $\cdot 10^{-4}$  mol) and AIBN (10.9 mg, 6.66  $\cdot 10^{-5}$  mol) were dissolved in 5 mL of DMF. The solution was stirred and bubbled with N $_2$  for 20 min, and a degassed solution of VAc (5.74 g, 6.66  $\cdot 10^{-2}$  mol) was injected. The septum was carefully replaced by a glass stopper and firmly closed with a keck joint clip. The solution was then stirred and heated at 70°C for 24 h. The viscous reaction was diluted with 5 mL of acetone and precipitated in a large excess of hexane. The resulting solid was dried until constant weight under vacuum at 40 °C (Yield = 88 %) (entry 8, Table 1). The equations used to determine the proportions of each type of PVAc chains (PVAc-CH $_2$ CH(OAc)-XA, PVAc-CH(OAc)CH $_2$ -XA, and PVAc-CH $_2$ -CH $_2$ (OAc) noted PVAc $_T$ -XA, PVAc $_H$ -XA and PVAc-H respectively) are detailed in SI. The attempted syntheses of PVDF-*b*-X (where X stands for NVP, BA and DMA) (entry 5, 6, 7 and 8, Table 1) were carried out using the same experimental protocol as the one used for the synthesis of PVDF-*b*-PVAc block copolymer



Scheme 1. Synthesis of PVDF-*b*-PVAc block copolymers.

#### DP and $M_{n(\text{NMR})}$ calculation

The degree of polymerization (DP) can be calculated from  $^1\text{H}$  NMR using the integrals of the signals corresponding to: the methyl group of the CTA R-group (1.19-1.24 ppm), the CH of PVAc backbone (4.76-5.14 ppm) and the CH $_2$  group end capped with xanthate moieties of the reverse VAc additions (HH, 3.22-3.46 ppm). However, as reported in a previous work,<sup>14</sup> the PVDF-XA chains initiated by R-radicals from the CTA were not all terminated by a CTA Z-group. Transfer to the DMC occurred in the course of the polymerization, leading to around 14 % of dead chains terminated by a -CF $_2$ H group. Therefore, a correction factor ( $\alpha = 0.86$ ) was introduced in equation (3) to

calculate a more accurate DP and molar mass for the PVAc block.

$$(1) \quad DP = \frac{\int_{4.76}^{5.14} \text{CH} + 1/2 \int_{3.22}^{3.46} \text{CH}_2(\text{HH End - group})}{\frac{\alpha}{3} \times \int_{1.19}^{1.24} \text{CH}_3 (\text{R - CTA}_{\text{XA}})}$$

The molar mass was then calculated using equation (2):

$$(2) \quad M_{n,\text{NMR}}(\text{R}) = M_{n,\text{PVDF-XA}} + (DP \times M_{n,\text{VAc}})$$

where  $M_{n,\text{PVDF}_{51}\text{-XA}} = 3500 \text{ g}\cdot\text{mol}^{-1}$ ,  $M_{n,\text{PVDF}_{85}\text{-XA}} = 5700 \text{ g}\cdot\text{mol}^{-1}$  and  $M_{n,\text{VAc}} = 86.09 \text{ g}\cdot\text{mol}^{-1}$ .

$^1\text{H}$  NMR (400 MHz ( $\text{CD}_3$ ) $_2\text{CO}$ ,  $\delta$  (ppm), Figure 1) : 1.19-1.24 (d, -CH( $\text{CH}_3$ )(C=O)-,  $^3J_{\text{HH}} = 7.1 \text{ Hz}$ ), 1.40-1.46 (t, (-S(C=S)O-CH $_2$ -CH $_3$ ), 1.63-1.92 (m, -CH(OAc)-CH $_2$ -CH(OAc)-, VAc), 1.92-2.03 (m, -CH(OAc)-, VAc), 2.28-2.43 (m, -CF $_2$ -CH $_2$ -CH $_2$ -CF $_2$ -, VDF-VDF TT reverse addition), 2.70-3.19 (t, -CF $_2$ -CH $_2$ -CF $_2$ -, regular VDF-VDF HT addition), 3.21-3.42 (m, -CH(OAc)-CH $_2$ -S(C=S)OEt, VAc HH reverse addition), 3.60-3.69 (s, -(C=O)-O-CH $_3$ ), 3.95-4.13 (-CH $_2$ -CH $_2$ (OAc), VAc), 4.63-4.72 (q, (-S(C=S)O-CH $_2$ -CH $_3$ ,  $^3J_{\text{HH}} = 7.2 \text{ Hz}$ ), 4.76-5.14 (-CH $_2$ -CH(OAc)-CH $_2$ -), 6.05-6.45 (tt,  $^2J_{\text{HF}} = 55 \text{ Hz}$ ,  $^3J_{\text{HH}} = 4.6 \text{ Hz}$  -CH $_2$ -CF $_2$ -H).

$^{19}\text{F}$  NMR (376 MHz ( $\text{CD}_3$ ) $_2\text{CO}$ ,  $\delta$  (ppm), Figure 2) : -115.63 (-CH $_2$ -CF $_2$ -CF $_2$ -CH $_2$ -CH $_2$ -, VDF-VDF HH reverse addition), -115.43 (-CH $_2$ -CF $_2$ -CF $_2$ -CH $_2$ -CH $_2$ -CH(OAc)-), -114.29 ( $^2J_{\text{HF}} = 55 \text{ Hz}$ , -CH $_2$ -CF $_2$ -H), -113.34 (-CH $_2$ -CF $_2$ -CF $_2$ -CH $_2$ -CH $_2$ -, HH reverse addition), -94.79 (-CH $_2$ -CH $_2$ -CF $_2$ -CH $_2$ -, TT reverse addition), -93.50 (-CH $_2$ -CF $_2$ -CH $_2$ -CH(CH $_3$ )(C=O)-), -92.12 (-CH $_2$ -CF $_2$ -CH $_2$ -CF $_2$ H), -91.44 (-CH $_2$ -CH $_2$ -CF $_2$ -CH $_2$ -CF $_2$ -CH $_2$ -CF $_2$ -, regular VDF-VDF HT addition), -91.00 (-CH $_2$ -CF $_2$ -CH $_2$ -, regular VDF-VDF HT addition).

#### Kinetic of PVDF-XA reactivation

A primary solution of VAc, PVDF macroRAFT agent, initiator and DMF targeting a desired DP was prepared and divided into various glass tubes previously purged with nitrogen. The tubes were then placed in a shaking oil bath thermostated at 70°C. The tubes were then taken off at different desired times and the reaction was quenched by immersion of the tube in liquid nitrogen. The crude product was then analyzed without purification by  $^1\text{H}$ ,  $^{19}\text{F}$  NMR and SEC. *In situ*  $^1\text{H}$  and  $^{19}\text{F}$  NMR experiments were achieved using a similar procedure. An aliquot of the required reaction mixture was placed in an NMR tube previously purged with nitrogen. Initial  $^1\text{H}$  and  $^{19}\text{F}$  NMR spectra were recorded at 25°C. The spectrometer was then heated at 70 °C, the NMR tube was then placed in the spectrometer and spectra were recorded every 2 minutes and 7 s for 5 hours using the above described acquisition parameters.

#### Computational details

The computational work was carried out using the Gaussian09 suite of programs.<sup>37</sup> The geometry optimizations were performed in the gas phase without any symmetry constraint using the B3PW91 functional in combination with the 6-31G(d,p) basis functions for all atoms. The unrestricted formulation was used for all radicals, yielding negligible spin contamination in all cases. The ZPVE, PV and TS corrections at 298 K were obtained with Gaussian09 from the solution of the

nuclear equation using the standard ideal gas and harmonic approximations at  $T = 298.15$  K, which also verified the nature of all optimized geometries as local minima or first order saddle points. A correction of 1.95 kcal/mol was applied to all  $G$  values to change the standard state from the gas phase (1 atm) to solution (1 M).<sup>38</sup> Geometry optimizations in solvent using the SMD polarizable continuum model<sup>39</sup> were also carried out for selected calculations (see Results section) in vinyl acetate ( $\epsilon = 4.2$ ) and in acetonitrile ( $\epsilon = 35.7$ ).

## Results and discussion

### Block synthesis tests

PVDF-XA macroCTAs featuring different chain-ends were first prepared according to published procedures (Table 1, entry 1-3).<sup>8</sup> As mentioned in our previous publications, the different  $\omega$ -chain-ends of these macroCTAs originate from the head-to-tail (HT) and head-to-head (HH) additions of VDF which lead to easily reactivated PVDF<sub>H</sub>-XA and much less reactive PVDF<sub>T</sub>-XA respectively, and from transfer to the solvent resulting in PVDF-H dead chains.<sup>8,9,35</sup> The synthesis protocols used in the present study (solution polymerization in DMC) cannot produce pure PVDF<sub>H</sub>-XA macroCTAs. The transfer reactions to the DMC are unavoidable. The formation of PVDF<sub>T</sub>-XA is intrinsic to the radical polymerization of VDF, and they accumulate in the reaction medium as the polymerization reaction progresses. It is possible to minimize the proportions of the PVDF<sub>T</sub>-XA less reactive chains by stopping the polymerization at low VDF conversion.<sup>35</sup> To probe the possibility of synthesizing block copolymers from PVDF<sub>T</sub>-XA, a range of monomers including *N*-vinylpyrrolidone (NVP, entry 5, Table 1), *N,N*-dimethyl acrylamide (DMA, entry 6, Table 1), butyl acrylate (BA, entry 7, Table 1), and vinyl acetate (VAc, entry 8, Table 1) were tested in RAFT polymerization in the presence of the PVDF<sub>T</sub>-XA macroCTA obtained from entry 1 (DP = 51). VAc and NVP are good examples of 'less activated' monomers (LAM) which polymerization can be controlled using xanthate CTAs.<sup>40</sup> *N,N*-dimethyl acrylamide is an example of 'more activated' monomers (MAM) which polymerization in the presence of xanthate CTAs was recently claimed to proceed with satisfactory control.<sup>10,41</sup> Butyl acrylate is also a 'more activated'

monomer and its polymerization cannot be controlled using xanthate CTAs. These two MAMs were thus tested to see if they PVDF-XA could be reactivated by their radicals. The polymerizations of these monomers were carried out for 24 h and the resulting crude polymers were analyzed by <sup>1</sup>H and <sup>19</sup>F NMR spectroscopies and SEC-HPLC (see Figures S1, S2 and S3 respectively). In the case of NVP, DMA and BA, PVDF<sub>T</sub>-XA did not take part in the polymerization reactions. This can be clearly seen by comparing the <sup>1</sup>H (Figure S1) and <sup>19</sup>F NMR (Figure S2) spectra of PVDF<sub>T</sub>-XA with those of the corresponding chain extension reaction products. In the <sup>1</sup>H NMR spectra, the well-defined triplet centered at 4.10 ppm of the VDF unit adjacent to the xanthate moiety did not disappear while the <sup>19</sup>F NMR resonances at -113.09 and -112.69 ppm corresponding to the ultimate and penultimate VDF units of the xanthate-terminated PVDF chains did not decrease in intensity relatively to the main PVDF signal at -91 ppm, and no new signal appeared. In addition, the GPC traces (Figure S3) of the polymer resulting from the chain extension of PVDF<sub>T</sub>-XA with NVP, DMA and BA are bimodal and feature broad dispersities ( $\mathcal{D} > 1.8$ ). These results demonstrate that the PVDF<sub>T</sub>-XA chains behaved as spectators during the free radical polymerizations of these monomers.

Interestingly, when the PVDF-XA macroCTA from entry 3, containing both PVDF<sub>T</sub>-XA (38 mol %) and PVDF<sub>H</sub>-XA (47 mol %), was used in a chain extension reaction with NVP (entry 17, Table 1), a block copolymer was formed. The <sup>19</sup>F NMR spectrum of this block copolymer (Figure S4) shows the complete disappearance of the signal of PVDF<sub>H</sub>-XA end group (at -71 ppm). This proves the total reactivation of this type of end-groups by exchange with PNVP\* radical and the formation of a

block copolymers. In this case as well, the signals at -113.09 and -112.69 ppm assigned to the ultimate and penultimate VDF units in PVDF<sub>T</sub>-XA remained unchanged (Figure S4). This experiment shows that only the PVDF<sub>H</sub>-XA macroCTA can be reactivated under these RAFT polymerization conditions. Consequently, the resulting polymer is a binary mixture of PVDF<sub>T</sub>-XA and PVDF-*b*-PNVP, the latter containing exclusively a -CH<sub>2</sub>CF<sub>2</sub>-NVP- moiety at the block junction. The unreacted PVDF chains can easily be seen on the GPC trace of the diblock copolymer (low molar mass shoulder in Figure S5).

**Table 1.** Experimental conditions and results for the synthesis of PVDF and the chain extension

Reactions conditions : (i) (entry 1-3) VDF homopolymerization,  $[I]/[CTA_{XA}] = 0.1$  with I = Trigonox 121 and  $CTA_{XA} = O\text{-ethyl-S-(1-methoxycarbonyl)ethylthiocarbonate}$ , T

Entry	CTA	M	$\frac{[M]_0}{[CTA]_0}$	Reaction time (h), Solvent	yield <sup>a</sup> (%)	DP <sub>(NMR)(R)</sub> <sup>b</sup>	M <sub>n(theo)</sub> <sup>c</sup> (g/mol)	M <sub>n(NMR)(R)</sub> <sup>d</sup> (g/mol)	M <sub>nSEC</sub> <sup>e</sup> (g/mol)	Đ <sup>e</sup>	End Group (%)					
											f	g	h	i	j	k
1	CTA <sub>XA</sub>	VDF	51	18, DMC	65	51	2400	3400	8300	1.40	86	0	14	n.a.	n.a.	n.a.
2	CTA <sub>XA</sub>	VDF	100	24, DMC	60	85	4100	5700	10100	1.50	49	0	51	n.a.	n.a.	n.a.
3	CTA <sub>XA</sub>	VDF	51	10, DMC	25	20	1000	1500	3900	1.12	38	47	15	n.a.	n.a.	n.a.
4	CTA <sub>XA</sub>	VAc	30	14, ACN	73	28	2100	2600	4000	1.20	n.a.	n.a.	n.a.	25	63	12
5	PVDF <sub>51</sub> -XA	NVP	150	24, DMF	80	n.a.	16800	n.a.	35500	2.10	86	0	14	n.a.	n.a.	n.a.
6	PVDF <sub>51</sub> -XA	DMA	100	24, DMF	73	n.a.	10700	n.a.	100000	1.79	86	0	14	n.a.	n.a.	n.a.
7	PVDF <sub>51</sub> -XA	BA	200	24, DMF	80	n.a.	24000	n.a.	58300	1.95	86	0	14	n.a.	n.a.	n.a.
8	PVDF <sub>51</sub> -XA	VAc	200	24, DMF	88	219	18600	22300	19100	1.40	0	0	14	33	0	53
9	PVDF <sub>51</sub> -XA	VAc	100	14, DMF	85	103	10800	12300	10200	1.41	0	0	14	36	0	50
10	PVDF <sub>51</sub> -XA	VAc	150	14, DMF	91	172	15200	18300	17500	1.34	0	0	14	35	0	49
11	PVDF <sub>51</sub> -XA	VAc	200	14, DMF	93	217	19500	22100	19500	1.39	0	0	14	40	0	46
12	PVDF <sub>51</sub> -XA	VAc	250	14, DMF	89	270	22700	26700	24200	1.35	0	0	14	32	0	54
13	PVDF <sub>51</sub> -XA	VAc	300	0.5, DMF	46	120	15300	13700	n.a.	n.a.	55	0	14	15	2	14
14	PVDF <sub>51</sub> -XA	VAc	300	3, DMF	59	238	18600	23900	17100	1.38	46	0	14	20	0	20
15	PVDF <sub>51</sub> -XA	VAc	300	6, DMF	73	273	22200	26900	22300	1.36	0	0	14	30	0	56
16	PVDF <sub>20</sub> -XA (Entry 3)	VAc	100	5, DMF	95	112	10000	11400	11300	1.33	5	0	15	53	5	22
17 <sup>l</sup>	PVDF <sub>20</sub> -XA (Entry 3)	NVP	200	14, DMF	50	n.a.	12600	n.a.	8000	1.98	n.a.	n.a.	n.a.	n.a.	n.a.	n.a.
18	PVDF <sub>85</sub> -XA (Entry 2)	VAc	250	14, DMF	65	318	17500	30100	18400	2.02	0	0	51	14	0	35

= 73 °C; (ii) (entry 4) VAc homopolymerization,  $[I]/[CTA_{XA}] = 0.1$  with I = AIBN and  $CTA_{XA} = O\text{-ethyl-S-(1-methoxycarbonyl)ethylthiocarbonate}$ , T = 60 °C; (iii) (entry 5-18) chain extension from PVDF-XA,  $[I]/[PVDF\text{-}XA] = 0.2$  with I = AIBN, T = 70 °C; <sup>a</sup>Determined gravimetrically. <sup>b</sup>Determined by <sup>1</sup>H NMR using equation (S1) for VDF and equation (1) for VAc. <sup>c</sup>Calculated using the yield as conversion and the equation:  $M_{n(theo)} = [M]_0/[CTA_{XA}]_0 \times \text{yield} \times M_n(M) + M_n(CTA_{XA})$ . <sup>d</sup>Calculated from DP<sub>NMR</sub> using equation (S2) for VDF and equation (2) for VAc. <sup>e</sup>Determined by SEC (RI detector). <sup>f</sup>-CF<sub>2</sub>-CH<sub>2</sub>-XA, calculated using equation (S3). <sup>g</sup>-CH<sub>2</sub>-CF<sub>2</sub>-XA, calculated using equation (S4). <sup>h</sup>-CF<sub>2</sub>H, calculated using equation (S5). <sup>i</sup>-AcOCH-CH<sub>2</sub>-XA, calculated using equation (S6). <sup>j</sup>-CH<sub>2</sub>-AcOCH-XA, calculated using equation (S7). <sup>k</sup>-CH<sub>2</sub>-AcOCH<sub>2</sub>, calculated using equation (S8). <sup>l</sup>The PNVP-XA end-groups could not be identified by <sup>1</sup>H NMR. However, since only PVDF<sub>H</sub>-XA were reactivated they should correspond to 38% of the total molar fraction of end-groups while PVDF<sub>T</sub>-XA and PVDF<sub>H</sub> correspond to 47 % and 15 % of end groups respectively. n.a.: not applicable.

### PVDF-*b*-PVAc block copolymers

In contrast with the above described chain extension attempts with NVP, DMA and BA, the chain extension of PVDF<sub>T</sub>-XA with VAc displayed a surprisingly narrow trace (Đ = 1.40, Figure S3), and a clear molar mass shift towards higher molar masses suggesting the formation of a relatively well-defined PVDF-*b*-PVAc block copolymer. Figure 1 displays the <sup>1</sup>H spectrum of the PVDF-*b*-PVAc block copolymer synthesized by chain extension of PVDF<sub>T</sub>-XA with VAc (entry 8, Table 1); and shows : (i) typical broad peaks centered at 1.75, 2.00, and 4.92 ppm corresponding respectively to the CH<sub>2</sub>, CH<sub>3</sub> and CH of PVAc, (ii) a broad triplet at 2.9 ppm assigned to the methylene of regular VDF head-to-tail (HT) additions and a triplet at 2.3 ppm characteristic of VDF tail-to-tail (TT) additions, (iii) signals assigned to the CTA R-group at 1.2 ppm (doublet) and 3.6 ppm

(singlet), (iv) signals of the CTA Z-group at 1.4 ppm (triplet) and 4.65 ppm (quartet), (v) a small peak centered at 3.3 ppm corresponding to a VAc head-to-head (HH) addition terminated by the xanthate group and, (vi) a triplet at 4.0 ppm characteristic of a -CH<sub>2</sub>-CH<sub>2</sub>(OAc) end-group caused by transfer of a -CH<sub>2</sub>CH(OAc)<sup>\*</sup> radical to the solvent.<sup>42,43</sup> Remarkably, the well-defined triplet at 4.10 ppm (coupling constant <sup>3</sup>J<sub>HF</sub> = 18 Hz) characteristic of PVDF<sub>T</sub>-XA chains, which remained unchanged when similar experiment were carried out with other monomers, completely disappeared in presence of VAc. This spectrum suggests the successful chain extension of PVDF<sub>T</sub>-XA by VAc.

This successful chain extension was further confirmed by comparing the <sup>19</sup>F NMR spectra of the polymers before and after chain extension with VAc (Figure 2).



The expanded  $^{19}\text{F}$  NMR spectrum between -112 and -116.3 ppm (inserts in Figure 2) clearly showed the shift of the signal at -112.69 ppm (assigned to the penultimate VDF unit) to -113.34 ppm. This signal at -113.34 overlaps with that of the VDF internal reverse (HH) addition. Similarly, the signal of the VDF ultimate unit (at -113.09 ppm) completely shifted to -115.43 ppm close to the second peak (at -115.63 ppm) of the VDF internal reverse (HH) addition. The signal integrals are also in very good agreement with these chemical shift changes. These shieldings are caused by the complete reactivation of the PVDF<sub>T</sub>-XA chains and with formation of the -CH<sub>2</sub>CF<sub>2</sub>CF<sub>2</sub>CH<sub>2</sub>-CH<sub>2</sub>CH(OAc)- linkage. A range of PVDF<sub>51</sub>-*b*-PVAc block copolymers with different PVAc block lengths was prepared (entry 9, 10, 11, and 12 in Table 1) from the PVDF<sub>T</sub>-XA macroC<sub>T</sub>A of entry 1. The corresponding viscosimetric GPC traces (Figure 3a) show narrow molar mass distributions ( $\text{Đ} < 1.4$ ) and an increase to high molar masses (in agreement with the PVAc chain length), indicating the quantitative reactivation of the reputedly inactive PVDF<sub>T</sub>-XA chains. Figure 3b displays the viscosimetric GPC traces of PVDF<sub>51</sub>-XA (entry 1, Table 1), PVDF<sub>85</sub>-XA, composed of 49 % PVDF<sub>T</sub>-XA and 51 % of -CF<sub>2</sub>H-terminated PVDF chains (PVDF-H) (entry 2, Table 1), and the diblock copolymers resulting from the chain extensions of these PVDF-XA macroC<sub>T</sub>As with VAc targeting a PVAc block length of 250 units and carried out under identical experimental conditions (entry 12 and 18, Table 1). The PVDF<sub>85</sub>-*b*-PVAc diblock copolymer is clearly of poor quality (high dispersity) and contains a significant amount of PVDF homopolymer (the completely unreactive PVDF-H chains formed by transfer to DMC<sup>8</sup> throughout the polymerization of VDF). In contrast, the chain extension of PVDF<sub>51</sub>-XA, which contained only 14 mol % of PVDF-H, led to a relatively well-defined block copolymer. The chain-end functionality of the starting PVDF macroC<sub>T</sub>A is thus a crucial parameter for the synthesis of well-defined PVDF-*b*-PVAc block copolymers.

### Reactivation Kinetics

PVDF<sub>T</sub>-XA chains are thermodynamically stable, hard to activate, and commonly considered as dead chains, whereas PVDF<sub>H</sub>-XA chains are considered as easily reactivatable by PVDF radicals. However, we have recently demonstrated that these considerations are wrong.<sup>35</sup>

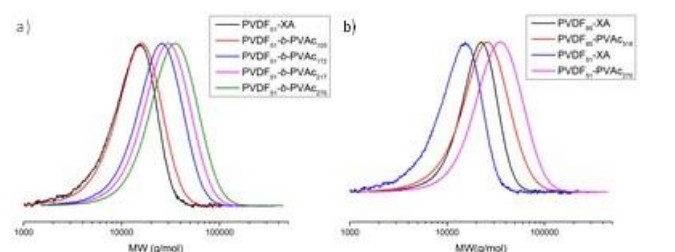


**Figure 3.** a) Normalized GPC traces (viscosimetric detector) of PVDF<sub>51</sub>-XA (entry 1, Table 1) homopolymer, PVDF<sub>51</sub>-*b*-PVAc<sub>103</sub> (entry 9, Table 1), PVDF<sub>51</sub>-*b*-PVAc<sub>172</sub> (entry 10, Table 1), PVDF<sub>51</sub>-*b*-PVAc<sub>217</sub> (entry 11, Table 1) and PVDF<sub>51</sub>-*b*-PVAc<sub>270</sub> (entry 12, Table 1) block copolymers, b) Normalized GPC traces (viscosimetric detector) of PVDF<sub>51</sub>-XA (entry 1, Table 1), PVDF<sub>85</sub>-XA (entry 2, Table 1), PVDF<sub>51</sub>-*b*-PVAc<sub>270</sub> (entry 12, Table 1) and PVDF<sub>85</sub>-*b*-PVAc<sub>318</sub> (entry 18, Table 1).

PVDF<sub>T</sub>-XA chains cannot be considered dead; they can be reactivated by PVDF<sub>T</sub><sup>\*</sup> and PVDF<sub>H</sub><sup>\*</sup> radicals, albeit at a slower rate than PVDF<sub>H</sub>-XA chains.

In the case of VDF RAFT homopolymerization, this reactivation slowdown leads to the accumulation of PVDF<sub>T</sub>-XA chains which ultimately leads to loss of the polymerization control. However, these chains can still be extended.

The reactivation kinetics of the two different type of PVDF-XA chains were examined using *in situ* NMR monitoring of the polymer chain-ends during the VAc chain extension of the PVDF<sub>20</sub>-XA macroC<sub>T</sub>A obtained from entry 3 (Table 1), composed of 38 % of PVDF<sub>T</sub>-XA, 47 % of PVDF<sub>H</sub>-XA and 15 % of PVDF-H. Figures S6 and S7 show, respectively, the stacked  $^1\text{H}$  and  $^{19}\text{F}$  NMR spectra of this PVDF-*b*-PVAc synthesis attempt. Figure 4 shows the evolution of the polymer chain-ends during this PVAc block synthesis experiment. These chain-ends monitoring revealed the extremely rapid reactivation of the PVDF<sub>H</sub>-XA chains and the much slower reactivation of the PVDF<sub>T</sub>-XA chains. The PVDF<sub>H</sub>-XA reactivation was already quantitative at only 11 % of VAc conversion (2 min and 7 s, second point in the *in situ* NMR monitoring in Figure 4) as evidenced by the total disappearance of the  $^{19}\text{F}$  NMR signal at -71 ppm and the appearance of a new signal at -93.14 ppm (Figure S8). After the same reaction time, the PVDF<sub>T</sub>-XA reactivation had reached only 7.6 %. The effect of the VAc target DP on the PVDF<sub>T</sub>-XA reactivation was also studied. Two PVDF<sub>51</sub>-XA chain extensions, targeting DP<sub>VAc</sub> = 100 and DP<sub>VAc</sub> = 300, were monitored by  $^1\text{H}$  and  $^{19}\text{F}$  NMR spectroscopies. The results of this study, summarized in Figure S10, did not reveal any significant influence of the targeted DP on the reactivation of the PVDF<sub>T</sub>-XA, although the reactivation seemed to complete at slightly lower conversions for the higher targeted DP.

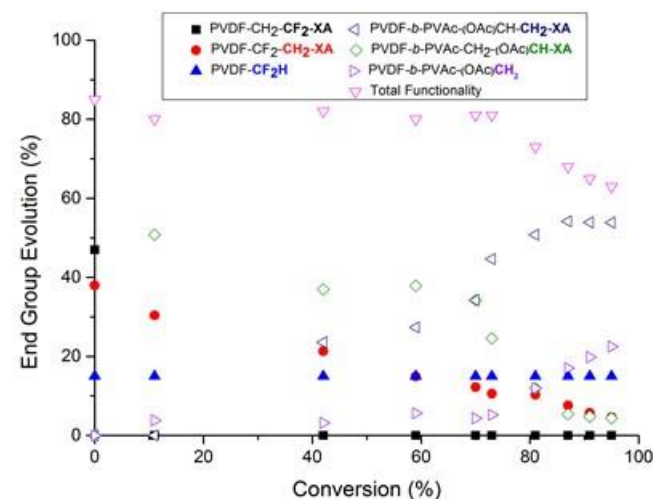


**Figure 4.** Evolution of chain-end functionality of PVDF<sub>20</sub>-*b*-PVAc during the PVAc block synthesis (target DP = 100) from PVDF<sub>20</sub>-XA (entry 3, Table 1) extracted from *in situ* NMR experiment. PVDF<sub>H</sub>-XA, PVDF<sub>T</sub>-XA, PVDF<sub>H</sub>-H designate PVDF-CH<sub>2</sub>CF<sub>2</sub>-XA, PVDF-CF<sub>2</sub>CH<sub>2</sub>-XA and PVDF-CH<sub>2</sub>CF<sub>2</sub>-H, respectively; and PVDF-*b*-PVAc<sub>H</sub>-XA, PVDF-*b*-PVAc<sub>T</sub>-XA, PVDF-*b*-PVAc<sub>H</sub>-H stand for PVDF-*b*-PVAc-CH<sub>2</sub>-CH(OAc)-XA, PVDF-*b*-PVAc-CH(OAc)-CH<sub>2</sub>-XA, PVDF-*b*-PVAc-CH<sub>2</sub>-CH(OAc)-H, respectively.

The much slower reactivation of this type of chain-end thus occurred throughout the polymerization and was actually still

incomplete when the NMR monitoring was stopped after 5h (5% of residual PVDF<sub>T</sub>-XA, Figure S9).

It is important to note that the RAFT polymerizations of VAc and VDF are very similar. In both cases monomer reverse additions (TT) lead to the accumulation of much less reactive species. For VAc, this has been mentioned in the past by several research groups but never studied in details.<sup>10,44</sup> We recently demonstrated that for PVDF, this accumulation is even faster and leads to a more pronounced broadening of the dispersity and slowdown of the degenerative chain transfer mechanism.<sup>35</sup> Figure 4 shows the fast accumulation of PVAc<sub>T</sub>-XA (-CH(OAc)CH<sub>2</sub>-XA-terminated PVAc chains) throughout the polymerization of VAc. At 42 % VAc conversion these PVAc<sub>T</sub>-XA already represent 37 % of the xanthate-terminated PVAc chains, and at 87 % VAc conversion, they represent 70 % of the xanthate-terminated PVAc chains. It is worth noting that at when VAc conversion reaches around 70 %, a surprising increase of transfer to solvent was observed. In consequence, the total functionality decreased drastically towards the end of the PVAc block synthesis (see Figure 4).

Figure 5 displays the evolution of the viscosimetric GPC traces of the PVAc block synthesis targeting DP<sub>VAc</sub> = 300 from a PVDF<sub>51</sub>-b-PVAc macroCTA (DP = 51, entry 1, Table 1) constituted only by PVDF<sub>T</sub>-XA and PVDF<sub>H</sub>-XA chains (PVDF<sub>T</sub>-XA/PVDF<sub>H</sub>-XA = 86/14). At Conv<sub>(VAc)</sub> = 46 %, a bimodal trace was observed. However, at higher conversions, the GPC traces appeared monomodal again and the dispersity did not increase significantly (initial Đ = 1.4, final Đ = 1.36). This surprising evolution may be explained by the chain inversions occurring during VAc polymerization and by the large amount of transfer to the solvent reactions. At Conv<sub>(VAc)</sub> = 46 %, only part of the starting PVDF<sub>T</sub>-XA has been reactivated (PVDF<sub>T</sub>-XA = 55% PVAc<sub>T</sub>-XA = 15%, PVAc<sub>H</sub>-XA = 2%) and the GPC trace is bimodal because it is the sum of the traces of the growing diblock copolymer and of the residual starting PVDF<sub>T</sub>-XA (and of the PVDF<sub>H</sub>-XA dead chains). As the polymerization carries on, the PVDF<sub>T</sub>-XA chains are gradually reactivated. Meanwhile, the PVAc growing block undergoes more and more chain inversion and PVAc<sub>T</sub>-XA accumulate in the polymerization medium. Indeed, at Conv<sub>(VAc)</sub> = 46%, the PVAc<sub>H</sub>-XA/PVAc<sub>T</sub>-XA ratio is = 10/90, and at higher VAc conversion (Conv<sub>(VAc)</sub> = 59% and 73%) the PVAc-XA segments are only composed of inversely added chain-ends (PVAc<sub>H</sub>-XA/PVAc<sub>T</sub>-XA = 0/100, Conv<sub>(VAc)</sub> = 59% : PVDF<sub>T</sub>-XA = 46% PVAc<sub>T</sub>-XA = 20%, PVAc<sub>H</sub>-XA = 0%, PVAc-H = 20% ; Conv<sub>(VAc)</sub> = 73% : PVDF<sub>T</sub>-XA = 0% PVAc<sub>T</sub>-XA = 30%, PVAc<sub>H</sub>-XA = 0%, PVAc-H = 56%). These PVAc<sub>T</sub>-XA chains tend to reactivate more slowly than the regularly-added chain-ends (PVAc<sub>H</sub>-XA). The PVAc block formed from slowly activating chains originating from PVDF<sub>T</sub>-XA, and thus likely terminated by a -CH<sub>2</sub>CH(OAc)-XA group (PVAc<sub>H</sub>-XA), grows faster than the polymer chains that have been reactivated before them but that have already been converted to the less reactive PVAc<sub>T</sub>-XA form.

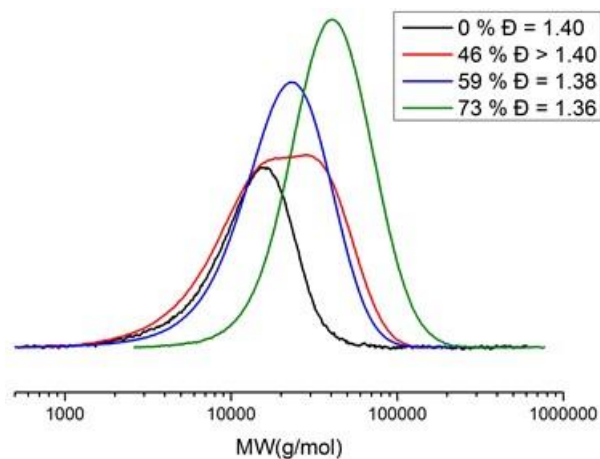


**Figure 5.** GPC traces scaled to Conv<sub>(VAc)</sub> (viscosimetric detector) of the PVDF<sub>51</sub>-b-PVAc block copolymers resulting from PVAc (target DP = 300) block synthesis from PVDF<sub>51</sub>-XA (entry 1 in Table 1: -CF<sub>2</sub>-CH<sub>2</sub>-XA/-CH<sub>2</sub>-CF<sub>2</sub>-XA/-CF<sub>2</sub>H = 86/0/14). Proportions of xanthate-terminated PVAc chains: red trace (entry 13, Table 1) Conv<sub>(VAc)</sub> = 46 %, PVAc<sub>H</sub>-XA/PVAc<sub>T</sub>-XA = 10/90 ; blue trace (entry 14, Table 1) Conv<sub>(VAc)</sub> = 59 %, PVAc<sub>H</sub>-XA/PVAc<sub>T</sub>-XA = 0/100, green trace (entry 15, Table 1) Conv<sub>(VAc)</sub> = 73 %, PVAc<sub>H</sub>-XA/PVAc<sub>T</sub>-XA = 0/100. Note: The determination of the molar mass and molar mass distribution of the diblock copolymers using GPC was not possible because it requires a concentration detector such as a RI detector; in the case of PVDF and PVAc, this cannot be used because of the negative response of PVDF and the positive response of PVAc in DMF. This is particularly true for the GPC trace corresponding to Conv<sub>(VAc)</sub> = 46 %.

In addition, the increasing amount of PVAc-H dead chains (formed by transfer reaction) observed at higher VAc conversion (PVAc-H = 56 % at VAc<sub>(Conv)</sub> = 73%) do not grow while the PVDF<sub>T</sub>-XA are still being reactivated. Consequently, the observed intermediate molar mass distribution broadening, eventually narrows down again. A thorough simulation of the RAFT polymerization of VDF, VAc and of the synthesis of PVDF-b-PVAc block copolymer using PREDICI will be undertaken in due time to test this hypothesis.

#### Assessment of the VAc chain transfer constant (C<sub>Tr</sub>) to PVDF<sub>H</sub>-XA and PVDF<sub>T</sub>-XA

The O'Brien and Gornick method,<sup>45</sup> previously used by Chong et al.<sup>46</sup> in the RAFT polymerization of styrene and by Boyer et al.<sup>47</sup> in the ITP of VDF, was employed to determine the apparent transfer constants C<sub>Tr(app)</sub> of the two types of PVDF macroCTAs (PVDF<sub>T</sub>-XA and PVDF<sub>H</sub>-XA) towards VAc. This simple method provides an estimate of the real transfer constants which are likely higher than the C<sub>Tr(app)</sub> determined here.<sup>47</sup>

Figures S11 and S12 show the plots of Ln([CTA]<sub>0</sub>/[CTA]) versus Ln([VAc]<sub>0</sub>/[VAc]) using data acquired from the *in situ* NMR experiments. Linear fitting of these plots provide the C<sub>Tr(app)</sub>, using equation (5):

$$(5) \quad \text{Ln}\left(\frac{[\text{CTA}]_0}{[\text{CTA}]}\right) = C_{\text{Tr}(\text{app})} \text{Ln}\left(\frac{[\text{VAc}]_0}{[\text{VAc}]}\right)$$

This simple method allows the determination of both C<sub>Tr(app)</sub> from the data of a single experiment. As mentioned earlier, the PVDF<sub>H</sub>-XA reactivation is extremely fast, yielding only two useful data points. The corresponding transfer constant was thus calculated to be at least 39 at 73 °C (Figure S11). In the case of the PVDF<sub>T</sub>-XA chains, which reactivated much more slowly, the *in-situ* NMR experiment yielded many more usable data points and the corresponding C<sub>Tr(app)</sub> was more accurately estimated at 0.8 at 73 °C (Figure S12). This large difference in the C<sub>Tr(app)</sub> of

the two types of PVDF macroCTAs confirms the observation that the PVDF<sub>H</sub>-XA chains reactivate much faster than the PVDF<sub>T</sub>-XA chains, but the latter is nonetheless reactivated at a significant rate. Indeed, 0.8 is very close to 1 which is considered as the theoretical limit value to achieve controlled polymerization (linear increase of the molar masses versus monomer conversion).<sup>48</sup> This value (which characterizes the radical transfer reaction from a vinyl acetate radical onto a PVDF<sub>T</sub>-XA macroCTA) is comparable to the chain transfer constant observed in the polymerization of styrene carried out in the presence of CTA<sub>XA</sub> ( $C_{Tr} = 0.67$  at 60 °C) and which does not afford narrow dispersity polystyrene ( $\bar{M}_w = 2.0$ ).<sup>49</sup> However, in the case presented here, this transfer only has to occur once; after reactivation and switch toward a VAc-terminated radical chain, the subsequent transfer reactions are those of the PVAc\* radicals under the RAFT operating conditions, which are known to afford adequate control ( $C_{Tr} = 25$  at 70 °C with CTA<sub>XA</sub> as RAFT agent and AIBN as initiator).<sup>50</sup>

### Thermal Analysis

The thermal stability of the new well-defined PVDF-*b*-PVAc block copolymers was determined by thermogravimetric analysis (TGA) in air. The thermograms are displayed in Figure S13. As described in a previous study,<sup>14</sup> PVDF-XA exhibited good thermal stability with no significant weight loss until 350 °C whereas PVAc-XA homopolymers start to decompose at 270 °C. The PVDF-*b*-PVAc block copolymers presented intermediate thermal stabilities between those of the PVDF and of the PVAc homopolymers, with no significant degradation below 310 °C. Differential scanning calorimetry (DSC) experiments were also performed, with specific attention to the PVDF crystallization. The corresponding DSC thermograms are shown in Figure 6. The PVDF<sub>51</sub>-XA exhibited a typical melting temperature at 170 °C. However, the expected PVDF glass transition at -40 °C<sup>33</sup> was not detected. In agreement with previous DSC studies on PVDF/PVAc blends,<sup>51</sup> complete disappearance of the melting temperature was noticed for the block copolymers (in PVDF-*b*-PVAc, with  $DP_{PVAc} > 100$ ). An exothermic transition was observed at 100 °C for PVDF<sub>51</sub>-*b*-PVAc<sub>103</sub>. This surprising phenomenon may be considered as a cold crystallization transition<sup>52</sup> probably caused by the higher PVDF content in this diblock compared to the other diblock copolymers examined. The disappearance of the PVDF melting temperature and the increase of the glass transition temperature with increasing PVAc weight fraction in PVDF-*b*-PVAc copolymers indicate the miscibility of PVDF and PVAc.

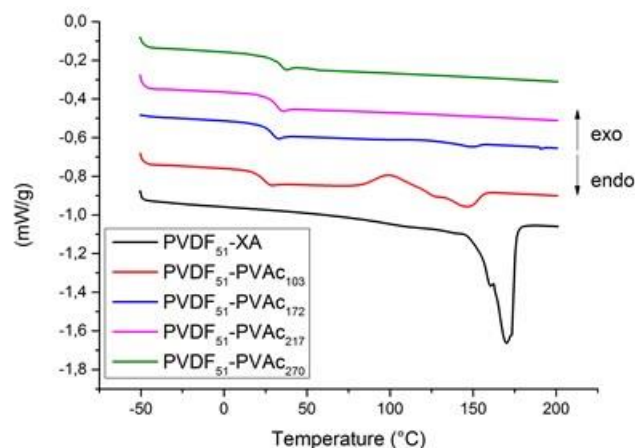


**Figure 6.** DSC thermograms (second heating) for: PVDF<sub>51</sub>-XA homopolymer (black), PVDF<sub>51</sub>-*b*-PVAc<sub>103</sub> (red), PVDF<sub>51</sub>-*b*-PVAc<sub>172</sub> (blue), PVDF<sub>51</sub>-*b*-PVAc<sub>217</sub> (pink) and PVDF<sub>51</sub>-*b*-PVAc<sub>270</sub> (green) block copolymers.

### Computational study

#### a. General considerations, choice of models and computation level

DFT calculations have amply provided insight into mechanistic issues associated to RDRP, particularly in RAFT,<sup>53</sup> ATRP,<sup>54</sup> OMRP,<sup>55</sup> and NMP.<sup>56</sup> The above described, partly unexpected experimental findings raised several mechanistic questions, the most important one being to understand which property makes VAc special for the reactivation of the less reactive PVDF<sub>T</sub>-XA dormant chains. In order to shed light on this phenomenon, DFT calculations were carried out on model systems. Related calculations on the homopolymerization of VDF by the RAFT method have been published by us in a recent article.<sup>35</sup> In order to keep the calculations manageable in terms of computational effort while obtaining results of indicative value, the polymer chains were simplified to an H atom beyond the terminal monomer unit.

Thus, the PVDF-CH<sub>2</sub>CF<sub>2</sub>\* (or PVDF<sub>H</sub>\*) and PVDF-CF<sub>2</sub>CH<sub>2</sub>\* (or PVDF<sub>T</sub>\*) chains were modeled respectively by CH<sub>3</sub>CF<sub>2</sub>\* and CHF<sub>2</sub>CH<sub>2</sub>\*, the PVAc-CH<sub>2</sub>CH(OAc)\* (or PVAc<sub>H</sub>\*) and PVAc-CH(OAc)CH<sub>2</sub>\* (or PVAc<sub>T</sub>\*) were modeled respectively by CH<sub>3</sub>CH(OAc)\* and (AcO)CH<sub>2</sub>CH<sub>2</sub>\*, and so forth. In the xanthate group, for the same reason of computational economy, the ethyl substituent in the xanthate group was simplified to a methyl group, -SC(S)OCH<sub>3</sub>. These structural modifications should not introduce major changes (polarity, homolytic strength, steric effects) in the bonds that are the focus of our investigations.

We stress that we do not aim at quantitatively reproducing observed data. The calculated energies associated to chemical reactions are rarely in agreement with the experimental ones by less than a couple of kcal/mol. Rather, the main objective of our computational approach is to provide insight into the occurring chemical processes. Energy trends within closely related systems are reproduced more faithfully than absolute values by the DFT calculations. For this reason, we have not tested different functionals and basis sets in order to find the most suitable method for our system. We have continued using B3W91/6-31G(d,p) as in our recent contribution on the closely

related VDF RAFT homopolymerization, allowing us to make direct comparisons between the two systems.<sup>35</sup> In that contribution, the method was benchmarked against the known VDF homopropagation rate constant and monomer inversion (head-to-head, or HH) errors, providing acceptable agreement between experimental and computational results. Additional benchmarking has now been carried out here on the VAc homopropagation process.

Experimental values, although showing much scatter depending on the investigation method, are available for the VAc propagation rate constant: 895, 1000 and 4600 M<sup>-1</sup> s<sup>-1</sup> in bulk at 25 °C,<sup>57</sup> 117 M<sup>-1</sup> s<sup>-1</sup> in benzene and 8 M<sup>-1</sup> s<sup>-1</sup> in benzonitrile.<sup>58</sup> From these values, standard activation free energies ( $\Delta G^\ddagger$ ) in the range 12.4-16.2 kcal/mol can be derived using the Eyring equation. The calculations for the CH<sub>3</sub>CH(OAc)\* addition to CH<sub>2</sub>=CH(OAc) to yield CH<sub>3</sub>CH(OAc)CH<sub>2</sub>CH(OAc)\* (regular head-to-tail (HT) addition) yield standard activation barriers ( $\Delta G^\ddagger$  298) of 17.6 kcal/mol from the gas phase calculations, 18.1 kcal/mol in bulk (vinyl acetate as solvent,  $\epsilon = 4.2$ ) and 18.1 kcal/mol in acetonitrile ( $\epsilon = 35.7$ ). We consider this agreement satisfactory, while the very small corrections observed for solvent models of disparate polarity, reflecting the uncharged nature of radicals, justified pursuing our exploration with the less time consuming and less problematic gas phase optimizations.

Another benchmarking was carried out on the basis of the VDF-VAc reactivity ratios, which were given in different contributions as 0.075±0.015 and 6±1 at 40°C in water,<sup>59</sup> and essentially zero (±0.04) and 1.67 (±0.6) at 45 °C in supercritical CO<sub>2</sub><sup>60</sup>, for  $r_{VDF}$  and  $r_{VAc}$ , respectively. From the calculated homo- and cross-propagation barriers restricted to the more favorable HT additions (*vide infra*) and the Eyring equation, the computationally predicted reactivity ratios are 0.06 and 1.8 at the operational polymerization temperature of 70 °C. Once again, the agreement can be considered satisfactory.

Comprehensive tables of energy and structural data for the geometry optimized molecules investigated in this study are provided in the Supporting Information (Tables S1 and S2, respectively).

### b. Bond strengths

Before presenting the results on the dormant chain activation processes, we briefly analyze the strength of the bonds linking the PVAc chain with the xanthate function. The calculated homolytic bond dissociation enthalpy (BDE,  $\Delta H^\circ_{298.15}$ ) for the CH<sub>3</sub>CH(OAc)-XA and CH<sub>2</sub>(OAc)CH<sub>2</sub>-XA bonds, models of the PVAc<sub>H</sub>-XA and PVAc<sub>T</sub>-XA chains, are respectively 48.7 and 55.6 kcal/mol, confirming the common perception that the bond is stronger in the T-terminated dormant species obtained after an inverted (HH) monomer addition. This situation parallels that reported for the CH<sub>3</sub>CF<sub>2</sub>-XA and CHF<sub>2</sub>CH<sub>2</sub>-XA bonds,<sup>35</sup> models of the PVDF<sub>H</sub>-XA and PVDF<sub>T</sub>-XA chains (54.5 and 60.7 kcal/mol). The BDE difference between the PVAc<sub>T</sub>-XA and PVAc<sub>H</sub>-XA models corresponds almost exactly to the energy difference of the isomeric radicals: the calculated standard enthalpy of CH<sub>2</sub>(OAc)CH<sub>2</sub>\* is 6.8 kcal/mol higher than that of CH<sub>3</sub>CH(OAc)\*. Consequently, the isomeric CTA models are essentially isoenergetic (CH<sub>3</sub>CH(OAc)-XA is more stable than CH<sub>2</sub>(OAc)CH<sub>2</sub>-XA by 0.4 kcal/mol), see Figure S14 where the energetic profile

of the related PVDF model systems<sup>35</sup> is also shown for comparison. Note that the BDEs values are greater for the VDF systems than for the VAc systems with equivalent terminal monomer orientation. This is consistent with the notion that the VDF radical (CH<sub>3</sub>CF<sub>2</sub>\*) is more reactive than the VAc radical (CH<sub>3</sub>CH(OAc)\*). Less expectedly, the BDE is also lower for VAc than for VDF when comparing the bonds generated by the tail monomer end, although both chain ends involve a primary methylene radical. This suggests that the  $\beta$ -C atom substituents (CF<sub>2</sub> vs. CH(OAc)) also have a significant influence on the radical stability and reactivity.

### c. VAc homopolymerization: radical exchange vs. propagation

The results of the calculations for the VAc homopolymerization are summarized in Figure 7. The Figure shows the energy profiles associated to the radical exchange process (chain transfer) in part a, and the addition to monomer (chain propagation) in part b. The scenario for the RAFT VAc homopolymerization is quite similar to that of the VDF homopolymerization.<sup>35</sup> The degenerative (HH and TT) and non-degenerative (HT and reverse TH) radical exchange processes go through associative PVAc-XA-PVAc radical intermediates, the energy of which is very close to those of the separate radical and dormant chain. The main difference relative to the VDF RAFT system is that all barriers are higher, both for the radical exchange and for the monomer addition processes. In terms of radical addition to monomer (Figure 7b), the regular H-CH<sub>2</sub>CH(OAc)\* radical (model of PVAc<sub>H</sub>\*) prefers the HT addition mode (blue profile in Figure 7b,  $\Delta G^\ddagger_{p,HT} = 19.6$  kcal/mol). The calculated  $k_{p,HT}/k_{p,HH}$  ratio is 5.8 at 70 °C which predicts a 15% probability of inverted monomer additions. The experimentally reported inverse addition frequency is in the 1-2 % range.<sup>44(b),61</sup> The PVAc<sub>T</sub>\* model radical species adds to monomer more favorably in the TT mode ( $\Delta G^\ddagger_{p,TT} = 15.2$  kcal/mol vs.  $\Delta G^\ddagger_{p,TH} = 19.0$  kcal/mol) to regenerate the regular chain-end (99.6% probability). The energy difference between the isomeric HH and HT (or TH and TT) products reflects the greater bond strength of CH(X)-CH<sub>2</sub> relative to CH(X)-CH(OAc) (X = H for the HT and HH addition; OAc for the TH and TT addition).

As previously found for the VDF RAFT system,<sup>35</sup> the barrier to the degenerative exchange between the regular PVAc<sub>H</sub>\* radicals on the xanthate CTA (blue profile in Figure 7a,  $\Delta G^\ddagger_{Exch,HH} = 11.4$  kcal/mol) is smaller than the monomer addition barrier, which is a necessary condition to insure good control by degenerative transfer. Application of the Eyring relationship yields the rate constants  $k_{p,HT} = 2.4$  M<sup>-1</sup> s<sup>-1</sup> for HT homopropagation and  $k_{Exch,HH} = 4.0 \cdot 10^5$  M<sup>-1</sup> s<sup>-1</sup> for the degenerative radical exchange at 70°C. Thus, the  $k_{Exch,HH}/k_{p,HT}$  ratio is 1.7·10<sup>5</sup>.

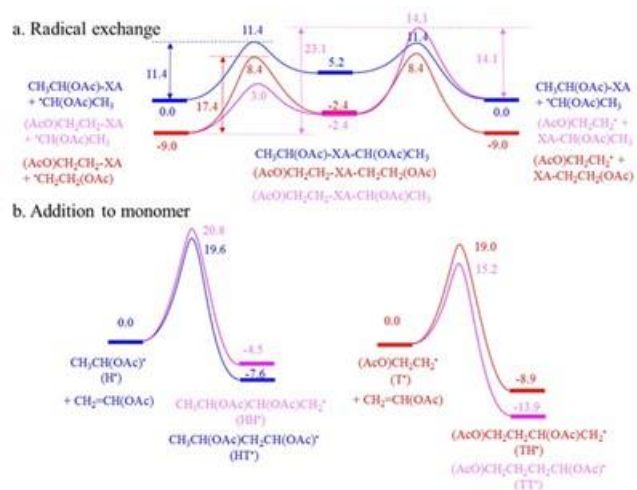


Figure 7. Energy profiles for (a) the degenerative (HH and TT) and non-degenerative (HT) radical exchange with the dormant chain and (b) for the different modes of radical addition to monomer in RAFT VAc homopolymerization. The reported values are ΔG (343.15 K) in kcal/mol.

The competing rates of the degenerative exchange and addition to monomer for the same radical depend not only on the rate constant ratio but also from the concentration ratio:

$$\frac{v_{\text{Exch,HH}}}{v_{\text{p,HT}}} = \frac{k_{\text{Exch,HH}}}{k_{\text{p,HT}}} \frac{[\text{PVAc}_H - \text{XA}]}{[\text{VAc}]}$$

which is in favor of the monomer and therefore favors propagation. However, even for high target DPs (e.g.  $[\text{VAc}]/[\text{PVAc-XA}] > 10^3$ ), the  $v_{\text{Exch,HH}}/v_{\text{p,HT}}$  ratio would still be in favor of exchange, guaranteeing controlled chain growth.

After an inverted monomer addition, the resulting PVAc<sub>T</sub>\* radical yield the more stable PVAc<sub>T</sub>-XA dormant chain by a thermodynamically favorable exchange with PVAc<sub>H</sub>-XA, which has a calculated barrier ( $\Delta G^{\ddagger}_{\text{Exch,HT}}$ ), for the model system, of 14.1 kcal/mol (pink profile in Figure 7a). Reactivation of this dormant chain with ultimate regeneration of the regular PVAc<sub>H</sub>\* radical requires release of the PVAc<sub>T</sub>\* radical from the dormant chain and TT monomer addition. This can be accomplished by exchange with the more abundant PVAc<sub>H</sub>\* radical (pink profile in Figure 7a,  $\Delta G^{\ddagger}_{\text{Exch,TH}} = 23.1$  kcal/mol) followed by TT addition to monomer. The profile involves a competing back-trapping (barrier of 14.1 kcal/mol,  $k_{\text{Exch,HT}} = 7.6 \cdot 10^3 \text{ s}^{-1} \text{ M}^{-1}$ ) and TT addition to monomer (barrier of 15.2 kcal/mol,  $k_{\text{p,TT}} = 1.5 \cdot 10^3 \text{ s}^{-1} \text{ M}^{-1}$ ) for the intermediate PVAc<sub>T</sub>\* radical. Although the rate constant is greater for back-trapping, the concentration factor ( $[\text{VAc}] > [\text{PVAc}_H - \text{XA}]$ ) is in favor of propagation. The complete rate expression for PVAc<sub>T</sub>-XA reactivation, under the steady state approximation for the PVAc<sub>T</sub>\* intermediate, is:

$$v_{\text{act}}(\text{PVAc}_T - \text{XA}) = \frac{k_{\text{Exch,TH}} k_{\text{p,TT}} [\text{PVAc}_H^*] [\text{PVAc}_T - \text{XA}] [\text{VAc}]}{k_{\text{Exch,HT}} [\text{PVAc}_H - \text{XA}] + k_{\text{p,TT}} [\text{VAc}]}$$

which under saturation conditions ( $[\text{VAc}] \gg [\text{PVAc}_H - \text{XA}]$ ) leading to faster propagation than back-trapping ( $k_{\text{p,TT}} [\text{VAc}] \gg k_{\text{Exch,HT}} [\text{PVAc}_H - \text{XA}]$ ) simplifies to:

$$v_{\text{act}}(\text{PVAc}_T - \text{XA}) = k_{\text{Exch,TH}} [\text{PVAc}_H^*] [\text{PVAc}_T - \text{XA}] = v_{\text{Exch,TH}}$$

This means that the reactivation of the PVDF<sub>T</sub>-XA dormant chain by the more abundant PVDF<sub>H</sub>\* radical is likely limited by the non-degenerative exchange ( $\Delta G^{\ddagger}_{\text{Exch,TH}} = 23.1$  kcal/mol,  $k_{\text{Exch,TH}} = 1.43 \cdot 10^2 \text{ s}^{-1} \text{ M}^{-1}$ ). On the other hand, for the VDF system, back-trapping was predicted faster than homopropagation, with a reactivation rate affected also by the subsequent propagation barrier.<sup>35</sup> The larger barrier for reactivation of PVDF<sub>T</sub>-XA relative to PVDF<sub>H</sub>-XA agrees with the polymerization slowdown and poorer control following the inverted monomer addition in the RAFT homopolymerization of VAc.<sup>62,63</sup>

It can also be imagined that the less abundant PVAc<sub>T</sub>\* radical contributes to the reactivation of the less reactive PVAc<sub>T</sub>-XA chains (red energy profile in Figure 7a,  $\Delta G^{\ddagger}_{\text{Exch,TT}}$  of 17.4 kcal/mol at 70°C). Indeed, in the recent VDF RAFT polymerization study,<sup>35</sup> the reactivation and chain extension of the PVDF<sub>T</sub>-XA chains (though with poor control) was shown to be dominated by the degenerative exchange with the less abundant PVDF<sub>T</sub>\* radical. The degenerative exchange

rate constant for the PVDF<sub>T</sub>-XA/PVDF<sub>T</sub>\* reaction is  $k_{\text{Exch,TT}} = 60.6 \text{ s}^{-1} \text{ M}^{-1}$ . However, the actual exchange rate has a first order dependence on the less abundant PVAc<sub>T</sub>\* radical concentration (estimated as 1-2 % of the total PVAc\* concentration from the experimentally known fraction of inverted monomers in the polymer chain). The relative rates of TT degenerative exchange and TH non-degenerative exchange for the same PVAc<sub>T</sub>-XA dormant chain can be calculated as:

$$\frac{v_{\text{Exch,TT}}}{v_{\text{Exch,TH}}} = \frac{k_{\text{Exch,TT}} [\text{PVAc}_T^*]}{k_{\text{Exch,TH}} [\text{PVAc}_H^*]}$$

Insertion of the rate constant ratio ( $4.2 \cdot 10^3$ ) and the above estimated radical ratio into this expression yields a rate ratio of 42-84. This suggests that, like in the recently reported VDF RAFT system and counterintuitively, the PVAc<sub>T</sub>-XA dormant chains are reactivated more rapidly by the degenerative exchange with the less abundant PVAc<sub>T</sub>\* radicals.

#### d. VDF/comonomer cross-exchange with xanthate and cross-propagation.

The investigation of the reactivation process of the PVDF-XA macroCTAs (PVDF<sub>H</sub>-XA, PVDF<sub>T</sub>-XA) in the block copolymerization experiments used the same approach described in the previous section: (i) determination of the Gibbs energy profile leading from the macroCTA models (CH<sub>3</sub>CF<sub>2</sub>-XA and CHF<sub>2</sub>CH<sub>2</sub>-XA, respectively) and the model of the active radical chain generated from the added monomer (CH<sub>3</sub>CH(OAc)\* for PVAc<sub>H</sub>\*, CH<sub>3</sub>CH(COOME)\* for PBA\*, CH<sub>3</sub>CHCO(NMe<sub>2</sub>)\* for PDMA\*, and CH<sub>3</sub>CH\*N(cyclo-COCH<sub>2</sub>CH<sub>2</sub>CH<sub>2</sub>) for PNVP\*) to the liberation of the desired CH<sub>3</sub>CF<sub>2</sub>\* or CHF<sub>2</sub>CH<sub>2</sub>\* free radical; (ii) investigation of the subsequent addition of these liberated radicals to the monomer of interest, yielding the chain-end switched new radical; (iii) analysis of the full energy profile with identification of the rate-limiting transition state of the overall process; (iv) derivation, through the Eyring relationship, of the effective rate constant for the macroCTA activation rate; (v) comparison with the activation barrier of the primary radical homopropagation. All the relevant results are collected in Table 2, in which the

Gibbs equilibrium and activation energies are reported at the polymerization temperature (70°C).

Figure 8 reports the results of the chain extension with VAc, limited to the reactivation by the more abundant  $\text{PVAc}_\text{H}^\bullet$  chains and of the addition of the resulting  $\text{PVDF}_\text{H}^\bullet$  and  $\text{PVDF}_\text{T}^\bullet$  model radicals to the tail end of the VAc monomer, yielding the HT and the TT coupled products, respectively. Complete energy diagrams including the activations by the minority  $\text{PVAc}_\text{T}^\bullet$  model and the  $\text{PVDF}_\text{H}^\bullet$  HH and TH additions to VAc are in the SI (Figures S15 and S16). As seen previously for the VDF<sup>35</sup> and above for the VAc homopolymerizations, the HH addition is less favored than the HT addition and the TH addition is less favored than the TT addition.

Activation of the regular chain-end model,  $\text{CH}_3\text{CF}_2\text{-XA}$ , has a large barrier ( $\Delta G^\ddagger_{\text{Exch}} = 19.4$  kcal/mol), the intermediate adduct fragmentation being the rate-limiting step. This barrier is much greater than those of the degenerative reactivations of  $\text{CH}_3\text{CF}_2\text{-XA}$  by  $\text{CH}_3\text{CF}_2^\bullet$  (10.6 kcal/mol),<sup>35</sup> and of  $\text{CH}_3\text{CH}(\text{OAc})\text{-XA}$  by  $\text{CH}_3\text{CH}(\text{OAc})^\bullet$  (11.4 kcal/mol, Figure 7a). However, contrary to these degenerative processes in VDF and VAc homopolymerizations, the subsequent addition of the  $\text{CH}_3\text{CF}_2^\bullet$  radical to the VAc monomer has a lower barrier ( $\Delta G^\ddagger_{\text{add}} = 11.6$  kcal/mol) than the back-trapping process ( $\Delta G^\ddagger_{\text{bt}} = 12.9$  kcal/mol). In addition, the concentration ratio ( $[\text{VAc}] \gg [\text{PVAc-XA}]$ ) plays further in favor of propagation. Therefore, once the  $\text{PVDF}_\text{H}^\bullet$  radical is generated, it is immediately transformed into a  $\text{PVAc}_\text{H}^\bullet$  radical which then undergoes RAFT homopolymerization according to the profile in Figure 7. Hence, the activation rate is limited by the non-degenerative exchange process with  $k_{\text{Exch}} = 3.2 \text{ M}^{-1} \text{ s}^{-1}$  for the  $\text{PVDF}_\text{H}\text{-XA}$  macroCCTA. This is actually a greater rate than for the reactivation of the  $\text{PVAc}_\text{T}^\bullet$

XA macroCCTA in VAc homopolymerization (*vide supra*) and is thus compatible with a fast reactivation process. It is also competitive with VAc homopropagation ( $\Delta G^\ddagger_{\text{p}} = 19.6$  kcal/mol). The relative rate of  $\text{PVAc}^\bullet$  addition to  $\text{PVDF}_\text{H}\text{-XA}$ , leading to macroCCTA reactivation, and addition to VAc, leading to homopropagation, is  $v_{\text{Exch}/\text{vp}} = (k_{\text{Exch}}/k_{\text{p}})([\text{PVDF}_\text{H}\text{-XA}]/[\text{VAc}])$ , with the rate constant ratio being 1.3. This is an important point, because the efficiency of chain extension depends on how rapidly the new radical can generate the chain from the macroCCTA before leading to significant homopropagation. The reactivation of the  $\text{PVDF}_\text{T}\text{-XA}$  macroCCTA by VAc involves, according to the calculations on the model system, a greater exchange barrier ( $\Delta G^\ddagger_{\text{Exch}} = 23.6$  kcal/mol), while TT coupling of the liberated  $\text{PVDF}_\text{T}^\bullet$  radical to VAc has a slightly greater barrier ( $\Delta G^\ddagger_{\text{add}} = 12.2$  kcal/mol) than back-trapping ( $\Delta G^\ddagger_{\text{bt}} = 11.0$  kcal/mol), yielding a rate constant ratio  $k_{\text{add}}/k_{\text{bt}} = 0.17$ .

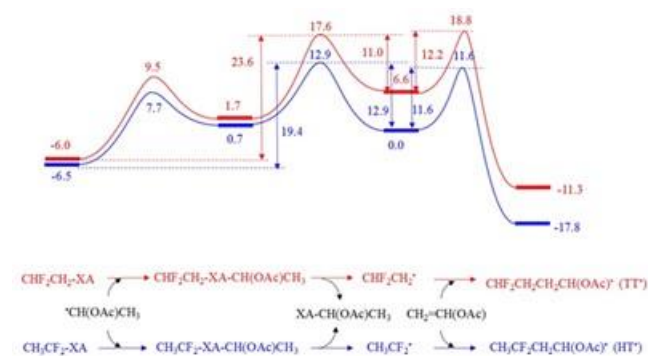


**Figure 8.** Energy profiles for the model  $\text{PVDF}_\text{H}\text{-XA}$  and  $\text{PVDF}_\text{T}\text{-XA}$  reactivation processes in the chain extension with VAc. The reported values are  $\Delta G$  (343.15 K) in kcal/mol, with the zero energy reference being the  $\text{CH}_3\text{CF}_2^\bullet$  radical.

**Table 2.** Summary of the calculated Gibbs energy changes for the propagation barriers, radical exchange and back-trapping barriers, radical exchange equilibrium, and addition of the liberated radical to monomer (in kcal/mol at 70°C), and predicted effective rate constants (in  $\text{M}^{-1} \text{ s}^{-1}$ ), for the reactivation of the  $\text{CH}_3\text{CF}_2\text{-XA}$  and  $\text{CHF}_2\text{CH}_2\text{-XA}$  macroCCTA models by different monomers.

MacroCCTA model	M <sup>a</sup>	$\Delta G^\ddagger_{\text{p}}^{\text{b}}$	$k_{\text{p}}^{\text{c}}$	$\Delta G^\ddagger_{\text{Exch}}^{\text{d}}$	$k_{\text{Exch}}^{\text{e}}$	$\Delta G^\ddagger_{\text{bt}}^{\text{c}}$	$\Delta G_{\text{Exch}}^{\text{f}}$	$\Delta G^\ddagger_{\text{add}}^{\text{g}}$	Experimental observations
$\text{CH}_3\text{CF}_2\text{-XA}$	VAc	19.6	2.4	19.4	3.2	12.9	6.5	11.6	Fast reactivation
$\text{CHF}_2\text{CH}_2\text{-XA}$				23.5	$8.0 \cdot 10^{-3}$	11.0	12.6	12.2	Slow reactivation
$\text{CH}_3\text{CF}_2\text{-XA}$	NVP	12.9	$4.4 \cdot 10^4$	21.4	0.17	9.5	11.9	11.0	Reactivation
$\text{CHF}_2\text{CH}_2\text{-XA}$				27.9	$1.3 \cdot 10^{-5}$	10.0	17.9	11.3	No reactivation
$\text{CH}_3\text{CF}_2\text{-XA}$	MA	16.0	$4.7 \cdot 10^2$	23.3	$1.1 \cdot 10^{-2}$	11.0	12.3	9.9	n.d. <sup>h</sup>
$\text{CHF}_2\text{CH}_2\text{-XA}$				28.1	$9.4 \cdot 10^{-6}$	9.7	18.4	11.4	No reactivation
$\text{CH}_3\text{CF}_2\text{-XA}$	DMA	17.1	94	17.2	81	1.0	16.2	10.7	n.d. <sup>h</sup>
$\text{CHF}_2\text{CH}_2\text{-XA}$				33.7	$2.6 \cdot 10^{-9}$	11.4	16.2	12.0	No reactivation

<sup>a</sup>Only the predominant addition of the liberated radical to the tail end of the monomer is considered. <sup>b</sup>Activation free energy for M homopropagation at 343.15 K. <sup>c</sup>Calculated from the corresponding  $\Delta G^\ddagger$  by the Eyring relationship at 343.15 K. <sup>d</sup>Activation free energy for the radical exchange from the macroCCTA model + H-M<sup>\*</sup> to H-M-XA and the macroradical model at 343.15 K. <sup>e</sup>Activation free energy for the back-trapping process leading from  $\text{CH}_3\text{CF}_2^\bullet$  or  $\text{CHF}_2\text{CH}_2^\bullet$  and H-M-XA to the starting macroCCTA model and HM<sup>\*</sup>. <sup>f</sup>Gibbs energy change for the radical exchange process at 343.15 K. <sup>g</sup>Activation barrier for the  $\text{CH}_3\text{CF}_2^\bullet$  or  $\text{CHF}_2\text{CH}_2^\bullet$  addition to M at 343.15 K. <sup>h</sup>n.d. = not determined.

However, like for the previously analyzed VAc homopolymerization, the concentration factor plays in favor of radical addition to monomer and thus the dormant chain activation is likely limited by the exchange process, yielding an estimated  $k_{\text{Exch}}$  of  $8.0 \cdot 10^{-3} \text{ M}^{-1} \text{ s}^{-1}$ . Hence, the regular PVDF<sub>H</sub>-XA macroCTA is reactivated 400 times faster than the PVDF<sub>T</sub>-XA macroCTA. This ratio is qualitatively consistent with the results of the apparent transfer constant determination (>39 and 0.3, Figures S11 and S12). In addition, since VAc homopropagation is now much faster ( $k_p = 2.4 \text{ s}^{-1} \text{ M}^{-1}$ ) than the macroCTA reactivation, the switching process is not predicted to lead to a diblock copolymer with a narrow molecular weight distribution. On the basis of the calculated rate constants, the ratio between propagation and activation rates is  $v_p/v_{\text{Exch}} = 300([\text{VAc}]/[\text{PVDF}_{\text{T}}\text{-XA}])$ , meaning for instance that for a  $[\text{VAc}]/[\text{PVDF}_{\text{T}}\text{-XA}]$  ratio of 100 as in entry 16, the PVAc\* radical should add on the average thirty thousand monomer molecules before activating the macroCTA. This is not in perfect agreement with the experiment since the PVDF-*b*-PVAc resulting from entry 8-16 (Table 1) have a relatively narrow molecular weight distribution, but the discrepancy can be rationalized not only by a possible computational overestimation of the activation barrier, greater than the overestimation of the propagation barrier, but also by the contribution to activation by the less abundant PVAc\* radicals (after an inverted VAc addition), since the activation barrier is in this case lower (19.8 kcal/mol, see Figure S16). The key to the reactivation of both PVDF<sub>H</sub>-XA and PVDF<sub>T</sub>-XA by VAc is that  $\Delta G_{\text{add}}^{\ddagger}$  is low for both head and tail PVDF\* radicals, i.e. the VDF-to-VAc monomer switch is faster than either VDF or VAc homopropagation.

#### e. Reactivation of PVDF-XA by NVP, BA and DMA.

The last question addressed by the DFT calculations is the failure of the NVP, BA and DMA monomers to afford well-defined block copolymers starting from the PVDF-XA macroCTA. As a reminder, neither of these monomers is able to extend the PVDF<sub>T</sub>-XA chains, but in case of NVP reactivation of the PVDF<sub>H</sub>-XA chains occurs.

Concerning the PVDF<sub>T</sub>-XA reactivation by NVP and by the other monomers, the exchange barriers are higher (27.9, 28.1 and 33.7 kcal/mol, respectively) than for the reactivation by VAc (23.5 kcal/mol, see Table 2). Furthermore, once activated, the back-trapping has a smaller activation barrier than the addition to monomer and the two processes will compete. The energy profiles for these reactivation processes are provided in the SI (Figure S17). From the calculated  $k_{\text{bt}}/k_{\text{add}}$  value (6.7 for NVP, 12 for MA, 2.4 for DMA), activation should still be limited by the exchange for high  $[\text{monomer}]/[\text{macroCTA}]$  ratios, but even in the most favorable case of an exchange-limited kinetics, the reactivation of PVDF<sub>T</sub>-XA by these monomers is at least two orders of magnitude slower than the reactivation by VAc (Table 2). These rates are much slower than those of homopropagation, thus once generated from the initiating  $\text{R}_0^*$  radicals, the new  $\text{R}_0\text{M}^*$  radicals lead to preferred homopropagation instead of exchange to release the PVDF\* radicals. This justifies the experimentally observed inability of these monomers to reactivate the PVDF<sub>T</sub>-XA chains.

Finally, for each monomer, the radical exchange involving the PVDF<sub>H</sub>-XA chains has a lower thermodynamic penalty by ca. 6 kcal/mol, than the radical exchange involving the PVDF<sub>T</sub>-XA chains according to the DFT calculations on the model systems. For NVP, the calculated exchange barrier is slightly higher (21.4 kcal/mol) than for the exchange involving VAc (19.4 kcal/mol) but lower than that of the PVDF<sub>T</sub>-XA reactivation by VAc (23.5 kcal/mol). The subsequent PVDF<sub>H</sub>\* addition to NVP, though having a slightly greater barrier (11.0 kcal/mol) than back-trapping, should not be rate-limiting because of the concentration factor as in the other situations examined above. This is consistent with the observed reactivation of PVDF<sub>H</sub>-XA by NVP. However, according to the calculations, the homopropagation of NVP is much faster than the exchange, contrary to the reactivation of PVDF<sub>H</sub>-XA by VAc, which yields faster exchange than homopropagation as shown above. This could in part rationalize the high dispersity of the PVDF-*b*-PNVP product (entry 17 in Table 1). The calculations also predict that it may be possible to reactivate the PVDF<sub>H</sub>-XA macroCTA with MA and DMA (see the data in Table 2 and the Gibbs energy profiles in Figure S18). This phenomenon has not been investigated experimentally since xanthate-based RAFT agents are known to poorly control the homopolymerization of acrylates or acrylamides.

## Conclusion

This article deals with the possibility of synthesizing block copolymers from PVDF-XA macroCTA via sequential addition of monomer. It shows that PVDF macroCTAs terminated by regularly added VDF unit (PVDF<sub>H</sub>-XA) are efficiently reactivated by both PVAc\* and PNVP\* radicals, thus leading to well-defined block copolymers. In contrast, PVDF macroCTAs terminated with an inversely added VDF unit (PVDF<sub>T</sub>-XA) were not reactivated by PNVP\* radicals. However, in the case of VAc, these less reactive PVDF<sub>T</sub>-XA macroCTAs are reactivated sufficiently fast to afford relatively well-defined PVDF-*b*-PVAc block copolymers. A thorough <sup>1</sup>H and <sup>19</sup>F NMR spectroscopic characterization of the block copolymers demonstrated this surprising complete reactivation of the reputedly “dead” PVDF<sub>T</sub>-XA chains. This difference in reactivation speed was confirmed by calculation of the corresponding transfer constants ( $C_{\text{Tr}} > 39$  for PVDF<sub>H</sub>-XA and  $C_{\text{Tr}} = 0.8$  for PVDF<sub>T</sub>-XA at 73 °C) using O’Brien and Gornick’s method. DFT calculations on model systems rationalize the observed behavior on the basis of differences in radical exchange kinetics ( $\Delta G_{\text{Exch}}^{\ddagger} = 19.4$  and 23.5 kcal/mol for PVDF<sub>H</sub>-XA and PVDF<sub>T</sub>-XA with VAc; 21.4 kcal/mol for PVDF<sub>H</sub>-XA with NVP), whereas the barriers for addition of the liberated PVDF<sub>H</sub>\* and PVDF<sub>T</sub>\* radicals to VAc and NVP are similar and yielding competitive addition rates relative to the thermodynamically favorable back-trapping. In addition, the macroCTA reactivation rates are competitive with the homopropagation rate of the chain extending monomer, particularly for the extension of PVDF<sub>H</sub>-XA with VAc. The lack of PVDF<sub>T</sub>-XA reactivation by NVP, BA and DMA is rationalized by

the fact that the rate of exchange is much lower than that of monomer homopropagation.

The thermal stability of the new PVDF-*b*-PVAc block copolymers was found to be intermediate between those of PVAc and PVDF homopolymers. DSC study of these block copolymers showed the complete disappearance of the crystallinity of PVDF and confirmed the miscibility of PVAc and PVDF. This work establishes, for the first time, efficient monomers sequential addition methods to synthesize unprecedented well-defined PVDF-*b*-PVAc block copolymers and gives detailed information on the mechanisms involved in the block extension steps. This work also opens the access to new PVDF-*b*-PVA amphiphilic block copolymer.

## Acknowledgements

The authors thank Arkema (Pierre Bénite, France) for providing VDF, and the French Ministry of Science and Technology for the Ph.D. grant attributed to MG.

## Notes and references

- B. Ameduri, B. Boutevin, *In Well-Architected Fluoropolymers: Synthesis, Properties and Applications*; Elsevier: Amsterdam, 2004.
- B. Ameduri, *Chem. Rev.*, 2009, **109**, 6632–6686.
- F. Boschet, B. Ameduri, *Chem. Rev.*, 2014, **114**, 927–980.
- M. Tatemoto, *In The First Regular Meeting of Soviet Japanese Fluorine Chemists*, Tokyo, 1979.
- (a) N. Durand, B. Ameduri, B. Boutevin, *J. Polym. Sci.: Part A: Polym. Chem.*, 2011, **49**, 82–92. (b) C. Boyer, D. Valade, L. Sauguet, B. Ameduri, B. Boutevin, *Macromolecules*, 2005, **38**, 10353–10362.
- B. Ameduri, *Macromolecules*, 2010, **43**, 10163–10184.
- (a) A. D. Asandei, O. I. Adebolu, C. P. Simpson, J. S. Kim, *Angew. Chem. Int. Ed.*, 2013, **52**, 10027–10030. (b) A. D. Asandei, *Chem. Rev.*, 2016, **116**, 2244–2274.
- M. Guerre, B. Campagne, O. Gimello, L. Parra, B. Ameduri, V. Ladmiral, *Macromolecules*, 2015, **48**, 7810–1822.
- M. Guerre, G. Lopez, T. Soulestin, C. Totée, B. Ameduri, G. Silly, V. Ladmiral, *Macromol. Chem. Phys.*, 2016, DOI: 10.1002/macp.201600109.
- S. Harrison, X. Liu, J.-N. Ollagnier, O. Coutelier, J.-D. Marty, M. Destarac, *Polymers*, 2014, **6**, 1437–1488.
- M. R. Hill, R. N. Carmean, B. S. Summerlin, *Macromolecules*, 2015, **48**, 5459–5469.
- S. Perrier, P. J. Takolpuckdee, *Polym. Sci.: Part A: Polym. Chem.*, 2005, **43**, 5347–5393.
- A. D. Asandei, O. Adebolu, C. P. Simpson, *J. Am. Chem. Soc.*, 2012, **134**, 6080–6083.
- M. Guerre, B. Ameduri, V. Ladmiral, *Polym. Chem.*, 2016, **7**, 441–450.
- V. S. D. Voet, G. ten Brinke, K. Loos, *J. Polym. Sci.: Part A: Polym. Chem.*, 2014, **52**, 2861–2877.
- Z. B. Zhang, S. K. Ying, Z. Q. Shi, *Polymer*, 1999, **40**, 1341–1345.
- S. M. Jol, W. S. Lee, B. S. Ahn, K. Y. Park, K. A. Kim, I. S. Rhee Paeng, *Polym. Bull.*, 2000, **44**, 1–8.
- M. Destarac, K. Matyjaszewski, E. Silverman, B. Ameduri, B. Boutevin, *Macromolecules*, 2000, **33**, 4613–4615.
- Z. Q. Shi, S. Holdcroft, *Macromolecules*, 2004, **37**, 2084–2089.
- Z. Q. Shi, S. Holdcroft, *Macromolecules*, 2005, **38**, 4193–4201.
- G. Laruelle, E. Nicol, B. Ameduri, J. F. Tassin; N. Ajellal, *J. Polym. Sci.: Part A: Polym. Chem.*, 2011, **49**, 3960–3969.
- K. Xu, K. Li, P. Khanchaitit, Q. Wang, *Chem. Mater.*, 2007, **19**, 5937–5945.
- C. Chanthad, K. A. Masser, K. Xu, J. Runt, Q. J. Wang, *Mater. Chem.*, 2012, **22**, 341–344.
- V. S. D. Voet, M. Tichelaar, S. Tanase, M. C. Mittelmeijer-Hazeleger, G. ten Brinke, K. Loos, *Nanoscale*, 2013, **5**, 184–192.
- V. S. D. Voet, D. Hermida-Merino, G. ten Brinke, K. Loos, *RSC Adv.*, 2013, **3**, 7938–7946.
- A. Meskini, M. Raihane, I. Stevenson-Royaux, G. Boiteux, G. Seytre, B. Ameduri, *J. Non-Cryst. Solids*, 2010, **356**, 688–694.
- G. David, C. Boyer, J. Tonnar, B. Ameduri, P. Lacroix-Desmazes, B. Boutevin, *Chem. Rev.*, 2006, **106**, 3936–3981.
- D. Valade, C. Boyer, B. Ameduri, B. Boutevin, *Macromolecules*, 2006, **39**, 8639–8651.
- G. Lopez, A. Thenappan, B. Ameduri, *ACS Macro. Lett.*, 2015, **4**, 16–20.
- a) P. Černoč, S. Petrova, Z. Černočová, J.-S. Kim, C. P. Simpson, A. D. Asandei, *Eur. Polym. J.*, 2015, **68**, 460–470. b) P. Černoč, Z. Černočová, S. Petrova, D. Kaňková, J.-S. Kim, V. Vasu, A. D. Asandei, *RSC Adv.*, 2016, **6**, 55374–55381.
- C. P. Simpson, A. I. Abdelou, J. S. Kim, V. Vasu, A. D. Asandei, *Macromolecules*, 2015, **48**, 6404–6420.
- G. Kostov, F. Boschet, J. Buller, L. Badache, S. Brandstadter, B. Ameduri, *Macromolecules*, 2011, **44**, 1841–1855.
- E. Girard, J.-D. Marty, B. Ameduri, M. Destarac, *ACS Macro Lett.*, 2012, **1**, 270–274.
- Y. Patil, B. Ameduri, *Polym. Chem.*, 2013, **4**, 2783–2799.
- M. Guerre, W. S. M. Rahaman, B. Ameduri, R. Poli, V. Ladmiral, *Macromolecules*, 2016, **49**, 5386–5396.
- X. Liu, O. Coutelier, S. Harrison, T. Tassaing, J.-D. Marty, M. Destarac, *ACS Macro Lett.* 2015, **4**, 89–93
- M. J. Frisch, G. W. Trucks, H. B. Schlegel, G. E. Scuseria, M. A. Robb, J. R. Cheeseman, G. Scalmani, V. Barone, B. Mennucci, G. A. Petersson, H. Nakatsuji, M. Caricato, X. Li, H. P. Hratchian, A. F. Izmaylov, J. Bloino, G. Zheng, J. L. Sonnenberg, M. Hada, M. Ehara, K. Toyota, R. Fukuda, J. Hasegawa, M. Ishida, T. Nakajima, Y. Honda, O. Kitao, H. Nakai, T. Vreven, J. A. Montgomery, Jr., J. E. Peralta, F. Ogliaro, M. Bearpark, J. J. Heyd, E. Brothers, K. N. Kudin, V. N. Staroverov, R. Kobayashi, J. Normand, K. Raghavachari, A. Rendell, J. C. Burant, S. S. Iyengar, J. Tomasi, M. Cossi, N. Rega, J. M. Millam, M. Klene, J. E. Knox, J. B. Cross, V. Bakken, C. Adamo, J. Jaramillo, R. Gomperts, R. E. Stratmann, O. Yazyev, A. J. Austin, R. Cammi, C. Pomelli, J. W. Ochterski, R. L. Martin, K. Morokuma, V. G. Zakrzewski, G. A. Voth, P. Salvador, J. J. Dannenberg, S. Dapprich, A. D. Daniels, Ö. Farkas, J. B. Foresman, J. V. Ortiz, J. Cioslowski, and D. J. Fox, *Gaussian, Inc.*, Wallingford CT, 2009.
- V. S. Bryantsev, M. S. Diallo, W. A. Goddard, III *J. Phys. Chem. B*, 2008, **112**, 9709–9719.
- A. V. Marenich, C. J. Cramer, D. G. Truhlar, *J. Phys. Chem. B*, 2009, **113**, 6378–6396.
- G. Moad, E. Rizzardo, S. H. Thang, *Aust. J. Chem.*, 2012, **65**, 985–1076.
- M. Destarac, D. Charmot, X. Franck, S. Z. Zard, *Macromol. Rapid. Commun.*, 2000, **21**, 1035–1039.
- W. R. Jr. Dolbier, *Fluorinated Free Radicals. Top. Curr. Chem.*, 1997, **192**, 97–163.
- J. Demarteau, A. Kermagoret, I. German, D. Cordella, K. Robeyns, J. De Winter, P. Gerbaux, C. Jerome, A. Debuigne, C. Detrembleur, *Chem. Comm.*, 2015, **51**, 14334.
- (a) Y. Kwak, A. Goto, T. Fukuda, Y. Kobayashi, S. Yamago, *Macromolecules*, 2006, **39**, 4671–4679. (b) A. N. Morin, C. Detrembleur, C. Jérôme, P. D. Tullio, R. Poli, A. Debuigne, *Macromolecules*, 2013, **46**, 4303–4312.
- J. L. O'Brien, F. Gornick, *J. Am. Chem. Soc.*, 1955, **77**, 4757.
- Y. K. Chong, J. Krstina, T. P. T. Le, G. Moad, A. Postma, E. Rizzardo, S. H. Thang, *Macromolecules*, 2003, **36**, 2256–2272.

- 47 ) G. Moad, E. Rizzardo, S. H. Thang, *Aust. J. Chem.* 2009, **62**, 1402. (b) E. Biccocchi, Y. K. Chong, L. Giorgini, G. Moad, E. Rizzardo, S. H. Thang, *Macromol. Chem. Phys.*, 2010, **211**, 529. (c) D. J. Keddie, C. Guerrero-Sanchez, G. Moad, R. J. Mulder, E. Rizzardo, S. H. Thang, *Macromolecules*, 2012, **45**, 4205.
- 48 C. Boyer, D. Valade, P. Lacroix-Desmazes, B. Ameduri, B. Boutevin, *J. Polym. Sci.: Part A: Polym. Chem.*, 2006, **44**, 5763-5777.
- 49 M. Adamy AM. van Herk, M. Destarac M. J. Monteiro, *Macromolecules*, 2003, **36**, 2293-2301.
- 50 P-E. Dufils, G. David, B. Boutevin, G. Woodward, G. Otter, A. Guinaudeau, S. Mazières, M. Destarac, *J. Polym. Sci.: Part A: Polym. Chem.*, 2012, **50**, 1997-2007.
- 51 R. Baskaran, S. Selvasekarapandian, N. Kuwata, J. Kawamura, T. Hattori, *Mat. Chem. and Phys.*, 2006, **98**, 55-61.
- 52 (a) Y. Chen, X. Chen, D. Zhou, Q. Shen, W. Hu, *Polymer*, 2016, **84**, 319-327. (b) J. You, H. Fu, W. Dong, L. Zhao, X. Cao, Y. Li, *ACS Appl. Mater. Interfaces*, 2012, **4**, 4825-4831.
- 53 (a) M. L. Coote, L. Radom, *J. Am. Chem. Soc.*, 2003, **125**, 1490-1491. (b) M. L. Coote, *Macromolecules*, 2004, **37**, 5023-5031. (c) M. L. Coote, L. Radom, *Macromolecules*, 2004, **37**, 590-596. (d) M. L. Coote, *J. Phys. Chem. A*, 2005, **109**, 1230-1239. (e) M. L. Coote, D. J. Henry, *Macromolecules*, 2005, **38**, 1415-1433. (f) M. L. Coote, D. J. Henry, *Macromolecules*, 2005, **38**, 5774-5779. (g) K. Matyjaszewski, R. Poli, *Macromolecules*, 2005, **38**, 8093-8100. (h) M. L. Coote, E. H. Krenske, E. I. Izgorodina, *Macromol. Rapid Comm.*, 2006, **27**, 473. (i) C. M. R. Abreu, P. V. Mendonça, A. C. Serra, J. F. J. Coelho, V. P. Anatoliy, G. Gryn'ova, M. L. Coote, T. Guliashvili, *Macromolecules*, 2012, **45**, 2200-2208.
- 54 (a) M. B. Gillies, K. Matyjaszewski, P-O. Norrby, T. Pintauer, R. Poli, P. Richard, *Macromolecules*, 2003, **36**, 8551-8559. (b) C. Y. Lin, M. L. Coote, A. Petit, P. Richard, R. Poli, K. Matyjaszewski, *Macromolecules*, 2007, **40**, 5985-5994. (c) W. A. Braunecker, W. C. Brown, B. Morelli, W. Tang, R. Poli, K. Matyjaszewski, *Macromolecules*, 2007, **40**, 8576-8585. (d) W. Tang, Y. Kwak, W. Braunecker, N. V. Tsarevsky, M. L. Coote, K. Matyjaszewski, *J. Am. Chem. Soc.*, 2008, **130**, 10702-10713. (e) Y. Zhang, K. Schröder, Y. Kwak, P. Krys, A. N. Morin, T. Pintauer, R. Poli, K. Matyjaszewski, *Macromolecules*, 2013, **46**, 5512-5519.
- 55 a) S. Maria, H. Kaneyoshi, K. Matyjaszewski, R. Poli, *Chem. Eur. J.*, 2007, **13**, 2480. (b) A. Debuigne, Y. Champouret, R. Jérôme, R. Poli, C. Detrembleur, *C. Chem. Eur. J.*, 2008, **14**, 4046-4059. (c) A. Debuigne, C. Michaux, C. Jérôme, R. Jérôme, R. Poli, C. Detrembleur, *Chem. Eur. J.*, 2008, **14**, 7623-7637. (d) Y. Champouret, U. Baisch, R. Poli, L. Tang, J. L. Conway, K. M. Smith, *Angew. Chem. Int. Ed. Engl.*, 2008, **47**, 6069-6072. (e) A. Debuigne, R. Poli, J. De Winter, P. Laurent, P. Gerbaux, P. Dubois, J-P. Wathelet, C. Jérôme, C. Detrembleur, *Chem. Eur. J.*, 2010, **16**, 1799-1811. (f) A. Debuigne, R. Poli, J. De Winter, P. Laurent, P. Gerbaux, J-P.; Wathelet, C. Jérôme, C. Detrembleur, *Macromolecules*, 2010, **43**, 2801-2813. (g) Y. Champouret, K. C. MacLeod, U. Baisch, B. O. Patrick, K. M. Smith, R. Poli, *Organometallics*, 2010, **29**, 167-176. (h) Y. Champouret, K. C. MacLeod, K. M. Smith, R. Poli, *Organometallics*, 2010, **29**, 3125-3132. (i) A. Debuigne, A. N. Morin, A. Kermagoret, Y. Piette, C. Detrembleur, C. Jérôme, R. Poli, *Chem. Eur. J.*, 2012, **18**, 12834-12844. (j) Y. Piette, A. Debuigne, C. Jérôme, V. Bodart, R. Poli, C. Detrembleur, *Polym. Chem.*, 2012, **3**, 2880-2891..
- 56 C. M. R. Abreu, P. V. Mendonça, A. C. Serra, B. B. Noble, T. Guliashvili, J. Nicolas, M. L. Coote, J. F. J. Coelho, *Macromolecules*, 2016, **49**, 490-498.
- 57 (a) W. J. Bengough, H. W. Melville, *Proc. R. Soc. London, Ser. A*, 1955, **230**, 429. (b) H. Kwart, H. S. Broadbent, P. D. Bartlett, *J. Am. Chem. Soc.*, 1950, **72**, 1060. (c) G. Dixon-Lewis, *Proc. R. Soc. London, Ser. A*, 1949, **198**, 510.
- 58 K. Kamachi, D. J. Liaw, S. Nozakura, *Polym. J.*, 1979, **11**, 921.
- 59 T. L. Latypov, A. A. Yul'chibayev, *Kuzieva Kh. Yu. Uzb. Khim. Zh.*, 1983, **62**.
- 60 B. Baradie, M. S. Shoichet, *Macromolecules*, 2002, **35**, 3569-3575.
- 61 P. J. Flory, F. S. Leutner, *Journal of Polymer Science*, 1948, **3**, 880. (b) D. Britton, F. Heatley, P. A. Lovell, *Macromolecules*, 1998, **31**, 2828.
- 62 K. Koumura, K. Satoh, M. Kamigaito, *Macromolecules*, 2009, **42**, 2497-2504.
- 63 K. Koumura, K. Satoh, M. Kamigaito, *Polymer Journal*, 2009, **41**, 595-603.

Table of Content:

